Dynamics of Precipitation Climatology

of the

Southwest Pacific Region

A THESIS

SUBMITTED IN PARTIAL FULFILMENT

OF THE REQUIREMENTS FOR THE DEGREE

OF

MASTER OF SCIENCE IN PHYSICS

IN THE

UNIVERSITY OF CANTERBURY

By

Ravinesh Chand Deo

Department of Physics & Astronomy

University of Canterbury

Christchurch, New Zealand

May 2001

Abstract

An analysis of ten-year mean precipitation data from 1990 – 1999 is presented, that examines precipitation trends for the western Pacific region, bounded by 155˚ E – 135˚ W, 15˚ N – 30˚ S. Wind fields derived from the NCEP/NCAR reanalaysis data are presented for the same period of study to examine the nature of the airflow for study region. To investigate the possible impacts of convergence and divergence on precipitation distribution, surface and 200 hPa divergence fields are derived using the wind fields and correlated with the precipitation data. Correlation between mean monthly Southern Oscillation Index (SOI) and precipitation is also carried out.

The precipitation patterns reveal several features that are prominent during the monthly and seasonal time scales. There is a rise in precipitation during highly negative surface divergences and a fall during positive surface divergences on the spatial map. It has been shown that summer shows the highest negative correlation between precipitation and surface divergence while autumn shows the least at the 5% level of significance. Correlation between SOI and precipitation indicates that highly positive correlation between the two variables exist along the zone of South Pacific Convergence Zone (SPCZ).

Acknowledgements

members of the department, who have assisted me in any way in completing my work. Big thank you to my nice flatmates, for giving me inspiration and moral support in the ups and down of the writing phase. You all are worthy of it!

Special thanks and appreciation goes to my best friend, Nilesh, for boosting my inspirations and for always being there to guide me. It was his belief that I will ultimately reach my goal – and I did. The completion of this thesis was certainly accelerated by the arrival of my fiancée, Aruna, so a very special acknowledgment to her for always wishing me good luck and success. Above all, my loving parents deserve the greatest hearty thanks, who have endured so much in educating me to this level, which would not have been possible without their prayers, wishes and hard work. Not forgetting my two brothers and the rest of my family who had always visualized their dreams through me, I thank them for their support. Thank you, My Lord for giving me the potentials to attain this level of education, which was not possible without your blessings.

Ravinesh C Deo
30 May 2001 ©

ॐ

In the name of the Almighty Lord

This work is dedicated to

Amma and Daddy

Contents

List of Figures

List of Tables

Chapter 1

Introduction

1.1 General Overview

Precipitation is an important component of the global hydrological cycle, which is probably the reason why it is such an important process for major human activities. In terms of the atmospheric processes that are modeled and predicted, it is probably the most difficult one to model or predict, due to the complexity of the underlying processes involved in its formation and occurrence. An understanding of climate dynamics is necessary to understand and explain precipitation occurrences and its varying patterns.

The precipitation fields in the southwest Pacific (bounded by 155˚ E – 135˚ W, 15˚ N – 30˚ S) show marked spatial and temporal variation due to the variable nature of the regions convergence zones, namely the Inter-tropical Convergence Zone (ITCZ), lying at about 5° N and the South Pacific Convergence Zone (SPCZ), which stretches in an east-southeasterly direction from Papua New Guinea across to Samoa and beyond (Basher and Zheng 1998). The amount of precipitation within the islands varies from 30 mm to 450 mm per month. Due to the shifts in the positions of the convergence zones, there is an inter-annual variation in rainfall patterns across the region. Associated with this is the El Niño Southern Oscillation (ENSO) phenomenon (Nicholls and Wong 1990), which is believed to be contributing to the precipitation variability within the region.

Salinger et al. (1995) state that for most of the southwest Pacific, climate records for the oceanic area are largely restricted to the tropical western half of the region where the populated island groups are located. An interesting feature of these stations is that they are

located at island sites, mainly on coral atolls, which are free from urban influences. This makes South Pacific climate data of particularly high quality for climate trend studies. For this reason, the analyzed data is of higher reliability and they can be used to assess the impacts of climate change in the southwest Pacific region.

Oort et al. (1992) emphasized the relation between the dynamics of atmospheric circulation and weather in the tropical regions. They stated that oceanic and atmospheric coupling plays a significant role in generating the different components of weather, such as wind and precipitation. The occurrence and intensity of precipitation, which is controlled by cloud microphysics and particle growth, as well as by regional patterns of pressure, temperature and humidity, needs more in-depth research. A thorough study of climate factors related to precipitation variability is extremely important for most of the developing nations in the region (Hulmes 1992). Khatep (1982) stated that in the New Zealand region, variations in precipitation amounts have important economic implications, especially in agricultural production and hydroelectricity generation. Similarly, for a developing nation like Fiji located within the southwest Pacific, agriculture plays the most significant role in its socio-economic development. The significant dependence of agricultural activities on the yearly amount of precipitation makes it an important issue to consider while studying climate trends. Basher and Zheng (1998) stated that the inter-annual rainfall variations due to ENSO are a major source of droughts and floods, which have a significant economic impact on the vulnerable small Pacific Island countries. Overall, an understanding of the climate dynamics is necessary for rainfall studies and is critical for effective planning and management of water and other scarce resources, which are the contributing factors to the development of any island nation.

The importance of studying precipitation patterns was given a global recognition in the 1995 Intergovernmental Panel for Climate Change (IPCC) Second Assessment, where global measured rainfall fields were used as a key test of the quality of those climate models used to predict climate changes arising from greenhouse gas emissions (Basher and Zheng 1998). Being given such an important aspect of climate change, precipitation studies has gained greater attention by the climatologists of the southwest Pacific island countries.

1.2 Aims

The aim of this thesis is to study the dynamics of regional atmospheric circulation and the precipitation patterns for the southwest Pacific region and to explain the variations in rainfall using current understanding of the circulation of the area.

The main objectives of this research are

- to provide an extensive background on the atmospheric circulation and precipitation patterns in the southwest Pacific region that currently exist
- to analyze measured rainfall data for the region and derive the broad spatial and temporal patterns of rainfall for monthly and seasonal trends
- to derive the horizontal divergence fields using surface and upper level wind fields and study the movement of the ITCZ and SPCZ using these horizontal divergence patterns
- to explain the variability of rainfall associated with the movement of the convergence zones on a monthly and seasonal scale
- to derive correlations between precipitation and the phases of the ENSO

1.3 Organization of the Thesis

This thesis is organized into 5 chapters. The various issues discussed in each of the chapters are as follows:

The current chapter has not only provided a general overview of the need to study precipitation patterns but has also defined the aims and objectives of the current research.

Chapter 2 gives the background knowledge of the rainfall patterns and atmospheric circulation patterns in the southwest Pacific region. Firstly, a brief climatology of the tropical Pacific region is presented including the dynamics and characteristics of the ITCZ and the SPCZ together with the seasonal circulation patterns of the southwest Pacific region. Furthermore, emphasis is given to the underlying physical processes involved in precipitation variability and the observed precipitation patterns of the region are discussed. Since precipitation variability is closely linked to the ENSO phenomenon, an account of ENSO related precipitation variability for the study region is provided.

Chapter 3 describes the characteristics of the precipitation data, including its source, spatial and temporal resolution and the analysis techniques adopted to produce precipitation patterns. Precipitation fields that are derived using the current dataset for the monthly and seasonal patterns are discussed with emphasis given to explaining various features that are evident in the plots. It continues with a description of the reanalysis wind data that was acquired to study the circulation patterns of the region. The monthly and seasonal surface wind fields, which demonstrate the possible positions of the convergence zones, are illustrated. The concept of continuity, which explains the role of surface and upper air divergence in relation to vertical atmospheric motion are introduced followed by a description of the procedure used to derive horizontal divergence fields for the study region. After presenting the horizontal divergence fields, precipitation contours are overlaid on them and any spatial correlation between them is noted. To quantify the relationship between surface horizontal divergence and precipitation, correlation analysis between the two variables is carried out. Furthermore, the latitudinal variability of precipitation and surface horizontal divergence are investigated. Correlations between monthly precipitation and ENSO events are carried out for stations located within the study region. Lastly, a synopsis of the results is provided which highlights the main findings of the research undertaken in this thesis.

Chapter 4 summarizes the outcomes of this research, and provides a synthesis of the results and literature work undertaken in this study. Lastly, it presents the conclusions of the study and recommendations that could be made for further research in this field of study.

Chapter 2

Atmospheric Dynamics and Precipitation Variability

2.1 Introduction

The dynamics of atmospheric motion, which occurs on a wide range of physical and temporal scales, governs all aspects of weather and climate. Since precipitation distribution is one of the major components of weather, studies regarding precipitation distribution have been a great concern for climate scientists over the past decades. As an issue of great concern for the islands located in the southwest Pacific region, many studies regarding precipitation patterns and its distribution have been done by climatologists such as Dourman and Bouke (1979), Taylor (1979), Rasmusson and Carpenter (1982), Philander (1990), Basher and Zheng (1995), Salinger (1995) and Basher and Zheng (1998).

Many important features of atmospheric circulation, including the radiation budget, convergence zones and seasonal circulation patterns significantly affect precipitation patterns over the southwest Pacific region. Therefore, it is vital that a short account of the climatology of the southwest Pacific region is presented before discussing the observed precipitation patterns that other researchers have previously identified. Due to the large influence of the El Niño Southern Oscillation (ENSO) phenomenon on precipitation (Sturman and McGowan 1999), the dependence of precipitation on ENSO is also considered.

2.2 Climatology of the Tropical Pacific Region

2.2.1 Significance of the Global Energy Budget

The driving force of all vertical and horizontal atmospheric motion is the incoming solar radiation, and the uneven distribution of the solar radiation across the globe is the driving force of the Earth's atmospheric circulation (Sturman and Tapper 1996). Illustrated in Figure 2.1 is the global distribution of solar radiation, measured at the top of the atmosphere. It shows that the central part of the Pacific receives net radiation of more than 80 Wm^{-2}, while regions north and south of about 40° experiences a net loss of radiation. Since the tropics have a surplus of radiation, sea surface temperatures (SST) are higher causing evaporation of water into the atmosphere. Given suitable conditions, the resulting humid air condenses and precipitates as rain. Studies conducted by Morrissey (1986) have verified that there are strong correlations between outgoing longwave radiation, atmospheric moisture level and precipitation. However, due to the uneven distribution of radiation, which is a function of time and location, the amount of precipitation varies geographically and temporally (Leroux 1998).
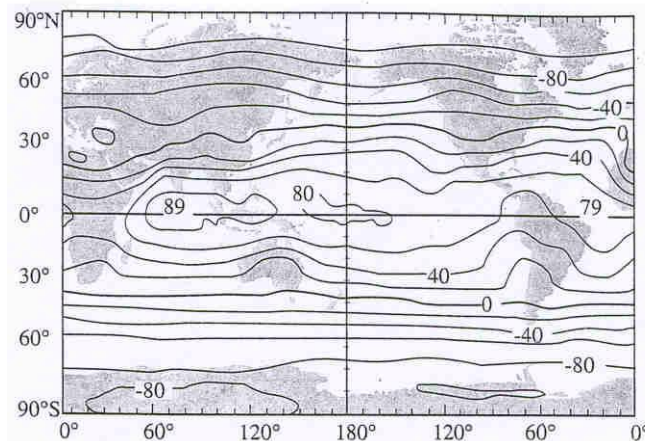
Figure 2.1   Global distribution of net solar radiation, measured at the top of the atmosphere (Wm^{-2}) (after Sturman and McGowan 1999).

2.2.2 Atmospheric Convergence Zones

The rainfall fields of the southwest Pacific region exhibit significant spatial and temporal variability due to the semi-permanent circulation features of the region, namely the Inter-tropical Convergence Zone (ITCZ) and the South Pacific Convergence Zone (SPCZ)

(Basher and Zheng 1998). Due to the important effect of these convergence zones on rainfall distribution, one must study their characteristics in order to understand their impacts on precipitation in the southwest Pacific region.

The ITCZ is an east-west belt that lies north of the equator and migrates from about 5° N in March and April to approximately 12° N in August and September. This is the region on the equatorial belt where the northeast and southwest trade winds converge (Horel 1982, Mitchell and Wallace 1992). As described by Hess et al. (1993), the ITCZ consists of a band of clouds of the order of few degrees of latitude in width. Thompson (1998) stated that the varying strength of the trade winds causes structural differences in the ITCZ. Incoming trade winds from both the hemispheres cause accumulation of moisture in the region of the ITCZ. Since convergence at the surface is associated with divergence at higher atmospheric levels, there is a vertical transport of moisture to higher levels in the atmosphere which results in clouds that later condense into rain. Weakly converging winds are associated with a poorly developed convergence zone with shallow cumulus clouds and little rain. Conversely, an intensified convergence within the ITCZ gives rise to torrential rain. However, more important than the ITCZ is the SPCZ, which has a direct effect on all major aspects of weather in the southwest Pacific region.

The SPCZ stretches in an east-southeasterly direction from Papua New Guinea into the central South Pacific region to about 30° S and 120° W. In its northwestern sector, the SPCZ becomes more horizontally oriented and merges with the ITCZ. The vast spatial and temporal extent of the SPCZ was not fully understood until satellite imagery became available in the early 1960s (Hubert 1961), even though it was first depicted in surface analyses of Bergeron (1930) (Vincent 1994). Many climalotogists including Trenberth (1976, 1991a), Streten and Zillman (1984), Kiladis et al. (1989) and Kodma (1992, 1993) have noted that the SPCZ lies in a region of low-level moisture convergence. Such a region has the potential to enhance precipitation formation and distribution in a similar way to the region of ITCZ. Meehl (1987) provided a convenient summary of the seasonal changes that occur within the region of the SPCZ, which relates to the seasonal variability of precipitation in the southwest Pacific region. Varying measures of convective activities progress eastward and southward in January into the SPCZ. Due to these progressions, the overall intensity of the SPCZ is greatest in January. Time series of monthly mean atmospheric parameters such as the wind, humidity, temperature and pressure fields show

minimum surface pressure anomalies, maximum cloudiness, minimum outgoing longwave radiation and maximum precipitation reaching the zonal portion of the SPCZ, near northern Australia, in January (Meehl 1987). They also show that lowest surface pressure and highest precipitation rates in the SPCZ region take place in austral summer. In light of these results, one can expect precipitation rates to be the highest during summer compared with other seasons for stations located within the vicinity of the SPCZ.

To study the variability of atmospheric convergence zones, many methods including satellite imagery (Philander 1990), analysis of cloud reflectivity data (Zheng at al. 1997) and derivation of surface horizontal divergences (Zheng et al 1997) have been carried out. Since surface horizontal divergence fields are derived to study the atmospheric convergence zones in this thesis, it is essential that previous studies undertaken by other climatologists be mentioned briefly. Zheng et al. (1997) produced weekly and monthly images of surface horizontal divergence fields using ERS-1 (European Remote Sensing-1) scatterometer data in the tropical Pacific region (120° E – 72° W, 30° N – 30° S). The data utilized here is of higher spatial and temporal resolutions owing to the fact that high resolution ERS-1 and NSCAT (NASA scatterometer) winds were available. Climatological images of surface horizontal divergence fields for 1992, 1993 and 1994 with weekly and monthly resolutions have verified that the positions of the ITCZ both in boreal winter and summer deviated 3 – 6° in latitude northwards from normal positions while the position of the SPCZ fluctuated with an amplitude as large as 10° in latitude. Rasmusson and Carpenter (1982) produced monthly mean (1949 – 1976) surface wind divergence fields over the area 30° N – 30° S for the months of February and August (Figure 2.2 & Figure 2.3). They reported that in February, the northeast trades extend westward across the north Pacific, merging in the western Pacific with the northeast flow of the Asian winter with maximum trade wind speeds of ~7 to 8 ms^{-1}. The ITCZ, located a few degrees north of the equator, is associated with a wind speed minimum with confluence and convergence in the surface wind field. However, in the Southern Hemisphere, the southeast trades are interrupted by the SPCZ, which is marked by cyclonic flow, convergence, confluence and speed minimum extending southeastward from the Solomon Islands. During August, the northeast trade winds are shifted several degrees northwards.

The question about the relationship between precipitation and surface horizontal divergence fields has been investigated by a number of authors, e.g. Bjerknes (1969), Cornejo-Garrido

8

(a)
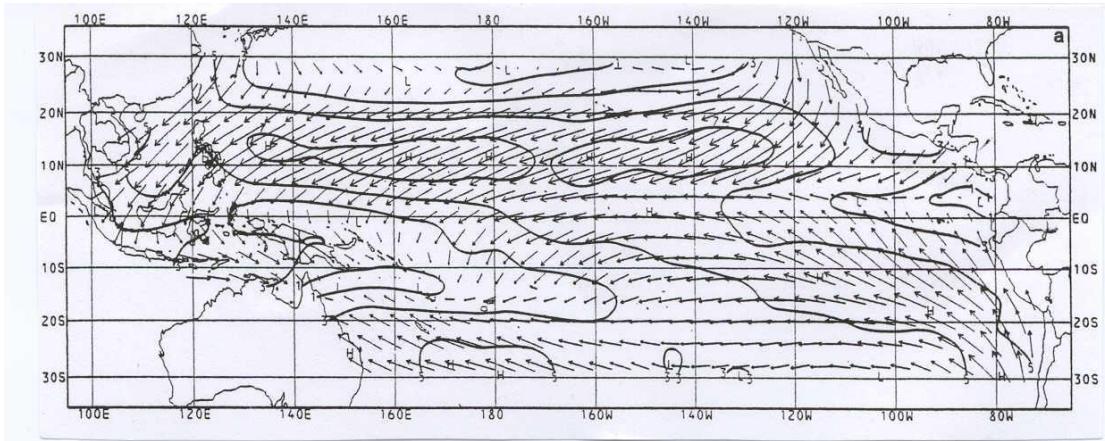
(b)
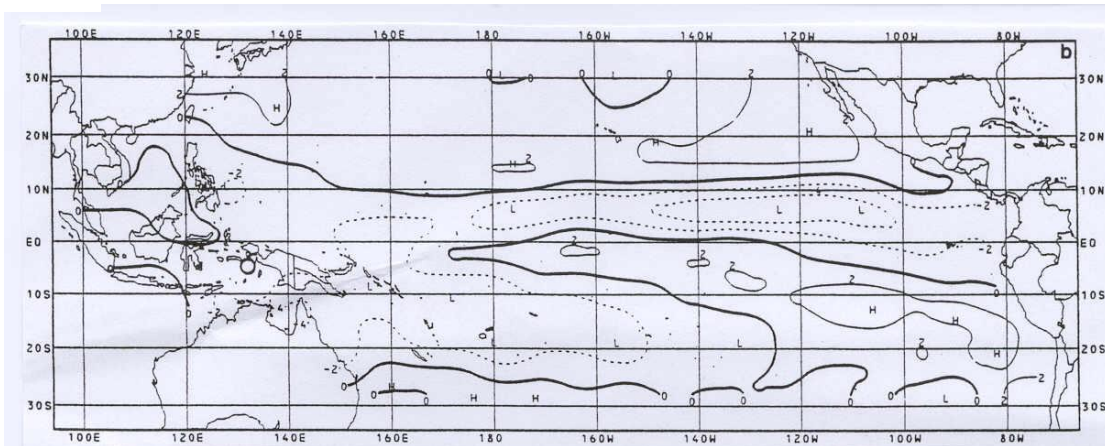
Figure 2.2 (a) Mean surface wind field and (b) velocity divergence for February. Units of isotachs are ms^{-1}; units of divergence 10^{-6} s^{-1}. Solid lines positive, dashed lines negative (after Rasmusson and Carpenter 1982).

and Stone (1977), Ramage et al. (1980), Rasmusson and Carpenter (1982) and McHugh (1999). Rasmusson and Carpenter (1982) has commented that the divergence anomaly composites together with typical values of specific humidity can be used to obtain an order of magnitude estimate of large-scale vapor flux divergence contribution. For example, taking mean values of divergence and specific humidity through to 150 mb as 2×10^{-6} s^{-1} and 14 g kg^{-1} respectively, the anomalous vapor flux convergence would be 110 mm month^{-1}, provided horizontal moisture gradients are neglected.. This value is similar to the amount of precipitation around the Canton Islands and he concluded that large-scale vapor flux convergence, rather than enhanced local evaporation serves as the main source of water vapor for enhanced precipitation. This shows the significance of vapor flux convergence in producing precipitation.

(a)

(b)
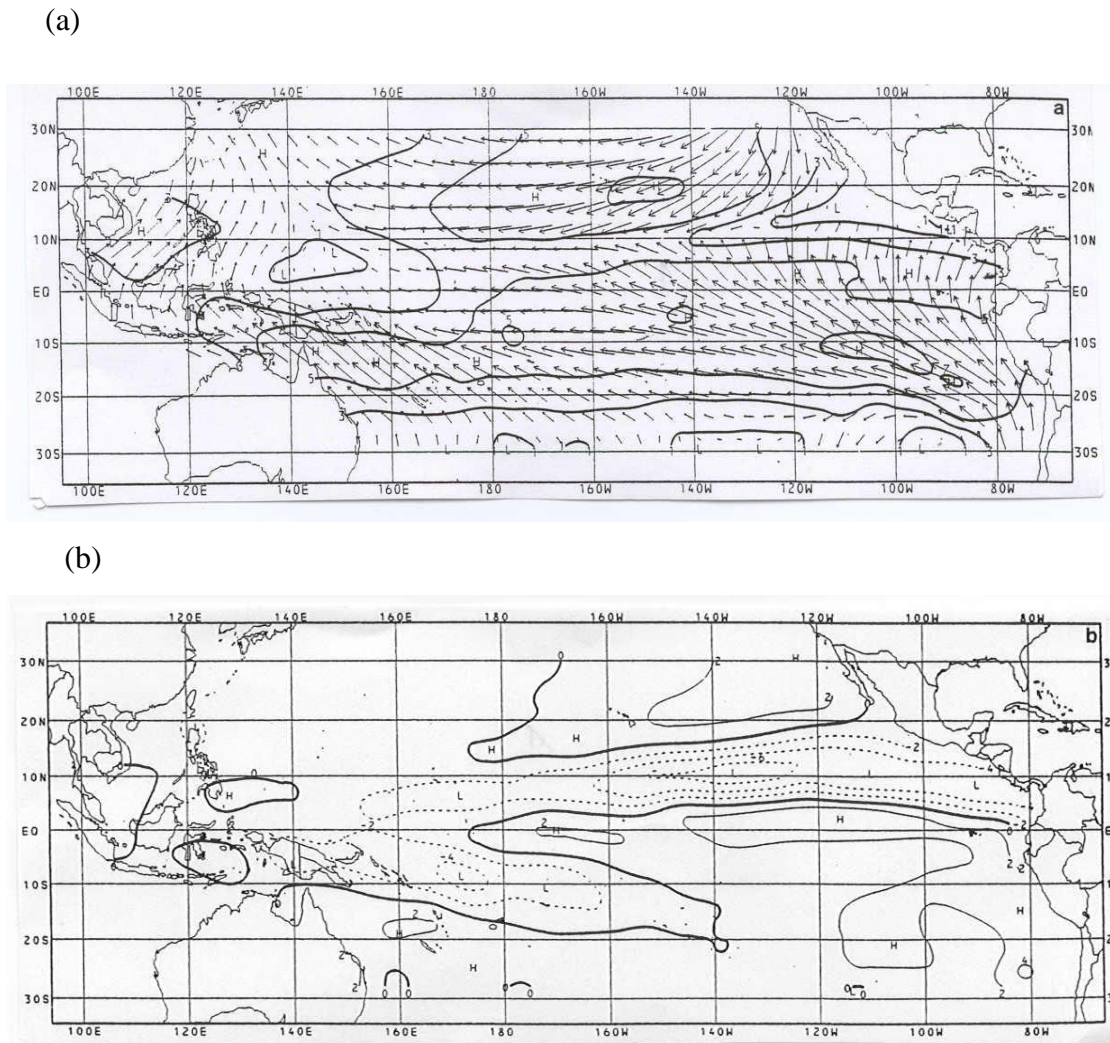
Figure 2.3 (a) Mean surface wind field and (b) velocity divergence for August. Units of isotachs are ms^{-1}; units of divergence 10^{-6} s^{-1}. Solid lines positive, dashed lines negative (after Rasmusson and Carpenter 1982).

2.3 Seasonal Circulation and Precipitation Patterns

2.3.1 January and July Circulation Patterns

Illustrated in Figure 2.4 are the main climatological features typical of the southwest Pacific region for January and July (or the middle months of summer and winter respectively). The striking features of January and July circulation are the trade wind regimes, the tropical convergence zones, sub-tropical high pressure belts and the westerlies to the south of the region (Salinger et al. 1995).

As discussed in the previous section, the ITCZ is located further southwards in January while it moves northwards in July. Following this movement, the SPCZ also shifts

southwards but to a smaller extent. The monsoonal trough, which is located in the northern Australia during January, vanishes in July. The southeast trades are more intense and dominant during July over much of the central southwest Pacific region. In the Northern Hemisphere during January, the trade winds are much stronger than the trades during July. High-pressure belts, which are located at about 40˚ S during January shift northwards due to the net shift in the whole pattern northwards in July. The northwesterly flow around Papua New Guinea that was due to the Australian monsoon in January disappears in July, when it replaced by southeasterly winds.

2.3.2   Precipitation Processes

Of the atmospheric processes predicted by numerical models, the precipitation produces by far the least satisfactory results (Sumner 1988). The limiting factor for this is the lack of data over oceans and mountainous areas. However, satellite sensors such as the Microwave Sounding Unit (MSU) are becoming increasingly useful tools to estimate precipitation over oceans and develop precipitation climatologies that could be merged with rain gauge measurements taken over land, to producing larger rainfall datasets over the whole globe (Spencer 1993). However, for studies that are focused on relatively small regions such as the South Pacific or the southwest Pacific, real time rain gauge measurements are more useful. Irregular data can be interpolated using appropriate geostatistical gridding methods, as used in the analyses of precipitation data in this research.

According to Hartmann (1994), precipitation is formed when air parcels become supersaturated with moisture which then leads to condensation and droplet formation. Three major types of precipitation in the tropics that occur over different geographical scales are convectional, cyclonic and orographic (McGregor 1998). Conventional rainfall is the result of free convection due to differential heating, dynamic processes such as convergence or physical forcing over mountains and it is characterized by considerable spatial variability. Cyclonic rainfall is due to horizontal convergence of moist air over in a circular area of low pressure where the vorticity maximum exists. This type of rainfall is typical during tropical cyclones. Orographic rainfall is the result of condensation or cloud formation in moist air due to physical barriers such as topography. Regardless of the type of rainfall, all rainfall is
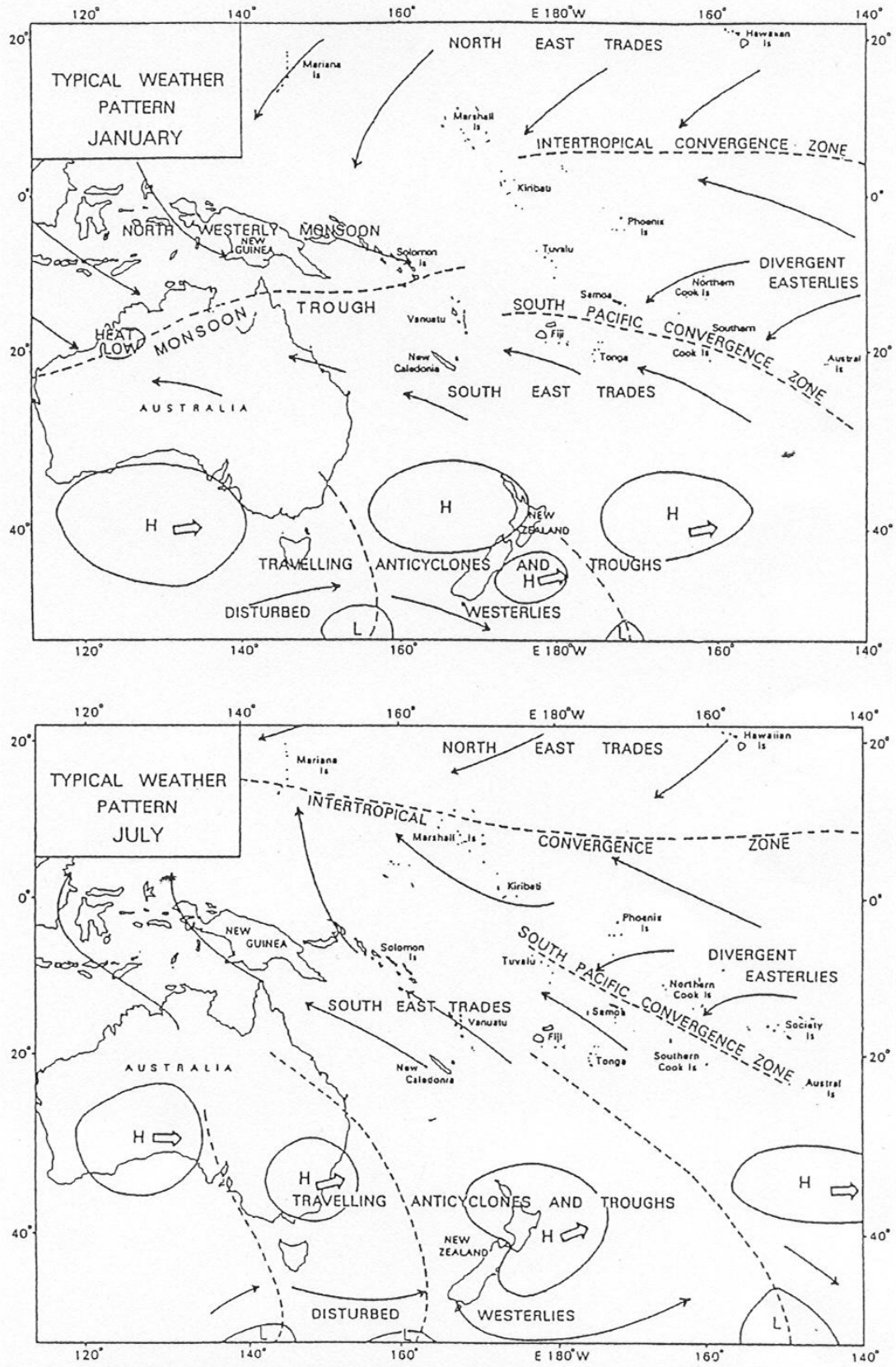
Figure 2.4   Typical features of the general circulation of the southwest Pacific region during January and July (reproduced from Steiner 1980).

12
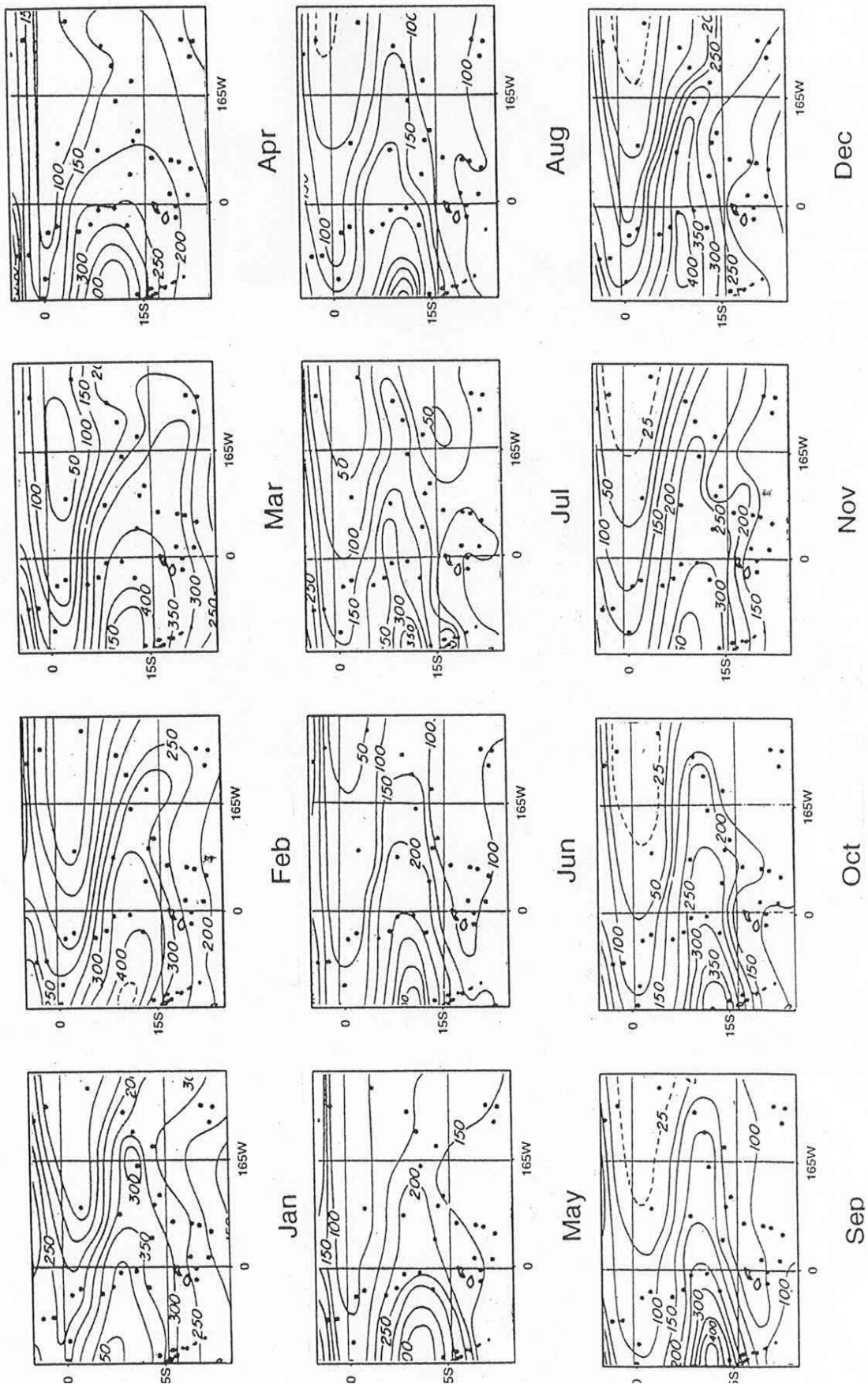
Figure 2.5 Manually derived map of average monthly rainfall (cm) for the central tropical Pacific Ocean (from Taylor 1973).

the result of vertical transport of moisture that occurs when the atmosphere is a state of conditional, potential or convective instability. Out of all these types of rainfall, this research is largely based on the study of convectional rainfall for the islands of the southwest Pacific region.

Previous studies of precipitation patterns over different geographical and temporal scales have verified that precipitation occurrence depends on a number of factors. Sumner (1988) has stated that much of the precipitation producing activity in the tropics occurs in the active areas of the equatorial trough, associated with the ITCZ and the SPCZ. Shin et al. (1990) studied the average precipitation for the tropical oceanic rainfall at the diurnal timescales. They have also reported that the ITCZ and the SPCZ have huge effect on precipitation occurrence, with SPCZ exhibiting significant power at diurnal and semi-diurnal frequencies in their data. Orographic precipitation is much more difficult to study than convectional precipitation due to the interaction of multiple factors such as the station altitude, station distance from the ocean, surface relief and the orientation of the elevation (Linarce 1992). However, Morrissey et al. (1993) stated that local terrain factors do not significantly affect precipitation on atolls, but for larger volcanic islands like Fiji, they do have an impact. The prevailing southeast trade winds produce a rainy windward and a drier leeward side on Fiji's main island, Viti Levu. Therefore, terrain factors are important for such volcanic islands of the southwest Pacific region.

2.3.3   Precipitation Patterns over the Southwest Pacific

Many climatologists have conducted previous studies into precipitation variability over the last three decades (Taylor 1973, Dorman and Bourke 1979, Rasmusson and Carpenter 1982, Zillman et al. 1989, Basher and Zheng 1995, Janowiak et al. 1995, Salinger et al. 1995 and Basher and Zheng 1998). A number of methods have been adopted to study precipitation variability due to its great spatial and temporal variability. Some such methods include in situ rainfall measurements taken by rain gauges or satellite estimates derived from cloud cover.

Illustrated in Figure 2.5 are the precipitation patterns for the tropical Pacific Ocean, derived manually by Taylor (1973). This was achieved by establishing isohyets between rainfall stations by means of satellite derived cloud cover patterns and gradients. The map illustrates

that the western part of the study region generally has more precipitation while the eastern part has less. The first four months of the year show highest precipitation amounts over the whole region while during May, June, July and August, amounts are severely with the lowest in July. From May to December, there is an increase in precipitation over the region again. Minimum values of precipitation are noted around the equator.
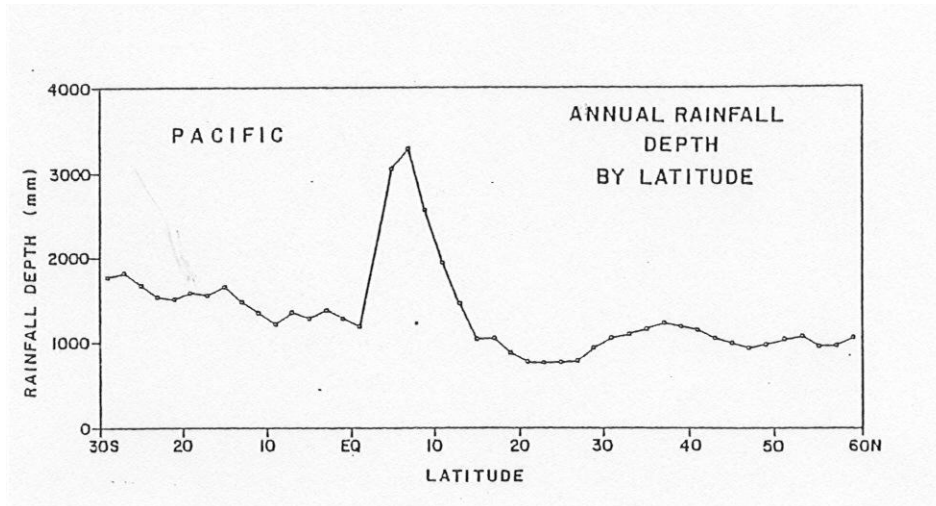
Figure 2.6   Mean annual depth (mm) using 2˚ latitude increments over tropical Pacific Ocean (from Dorman and Bourke 1979).

Dorman and Bourke (1979) mapped rainfall over the Pacific Ocean by using present weather observations and relating them to a given amount of precipitation and then deriving new estimates of oceanic rain between 30˚ S and 60˚ N. Presented in Figure 2.6 is the mean annual rainfall depth using 2˚ latitude increments over the Pacific Ocean. The narrow peak of 3400 mm at 7˚ N is a reflection of the ITCZ while to the south of the equator, rainfall increases slowly with a increase in latitude. The seasonal patterns derived by Dorman and Bourke (1979) indicate that in the extra-tropical northern Pacific, maxima occur in the fall and minima in the summer while in the South Pacific, maximum rainfall occurs in local summer (December-January-February). In the tropics (close to the equator), they have shown that maximum rainfall occurs in June through August.

Rasmusson and Carpenter (1982) demonstrated that the surface convergence fields not only show the characteristics of the ITCZ and SPCZ, but they can be also used to estimate rainfall. Their results indicate that the southward shift of the ITCZ in the austral summer is accompanied by a northward shift of the SPCZ, resulting in a smaller wedge-shaped dry zone and enhanced precipitation in the eastern and central tropical Pacific. Their sample
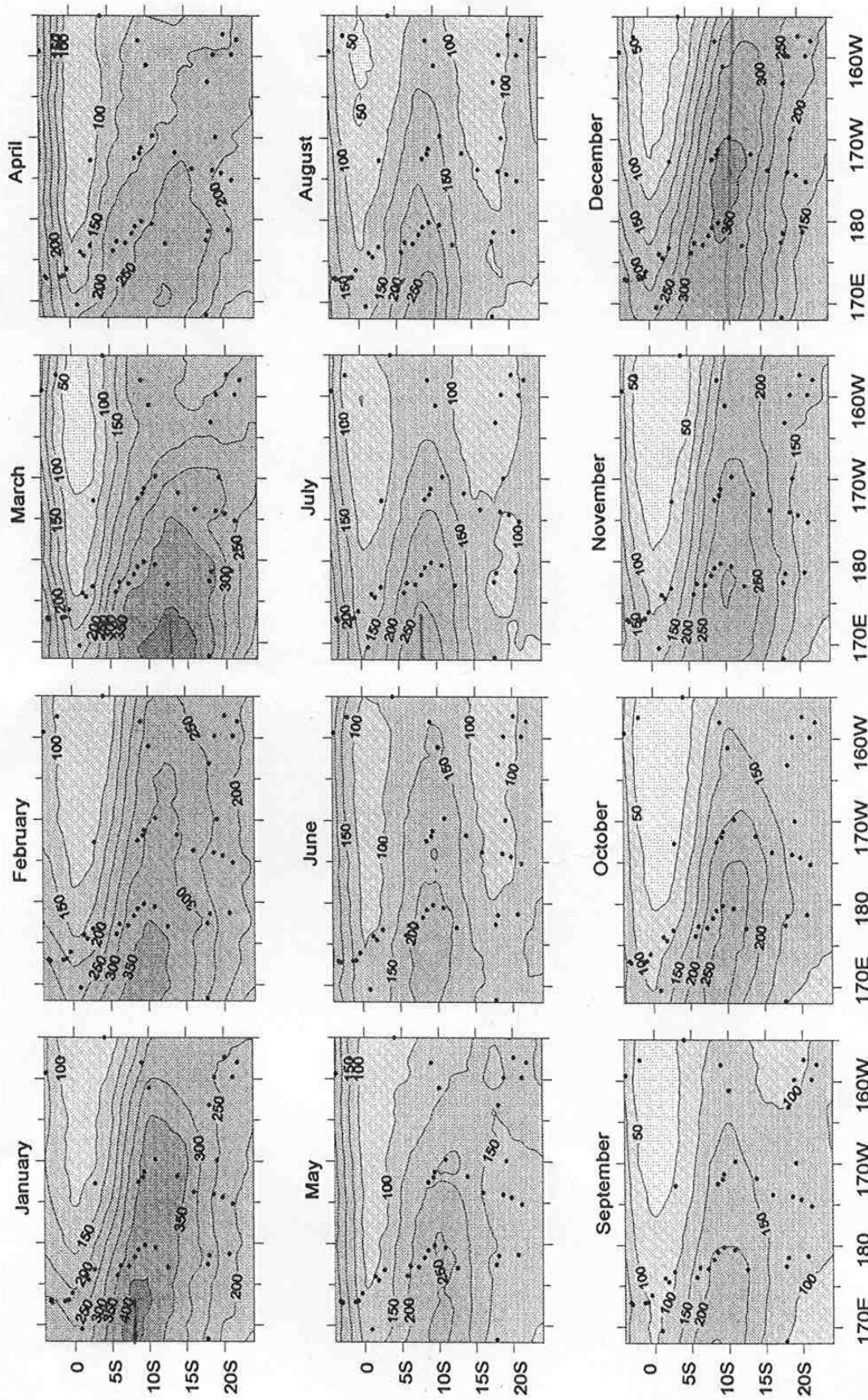
Figure 2.7 Mean monthly rainfall (cm) fields for the southwest Pacific, 1950-1989, computed by partial thin –plate spline fitting method with Outgoing Longwave Radiation (OLR) as the regression covariate (from Basher and Zheng 1998).
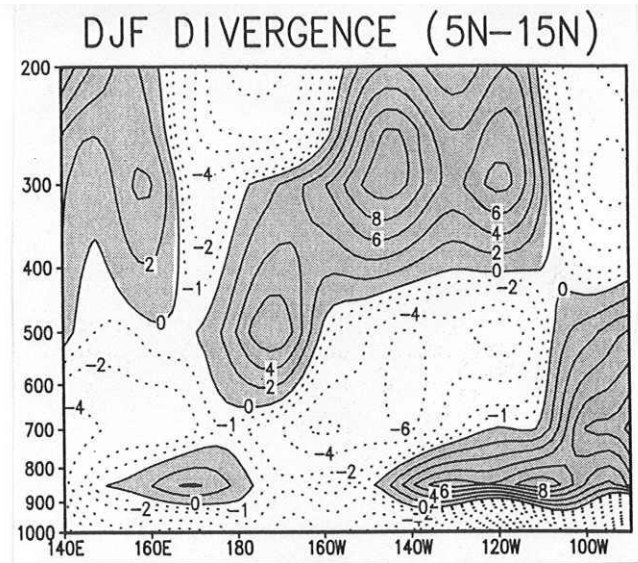
Figure 2.8a Longitude-height section of divergence for December-January-February derived from the NMC global data assimilation system averaged over 5˚ - 15˚ N to represent the Pacific ITCZ region. Shaded area indicates divergence, dotted area indicates convergence, and units are 10^{-7} s^{-1} for divergence and mb for heights (Source: Janowiak et al. 1995).
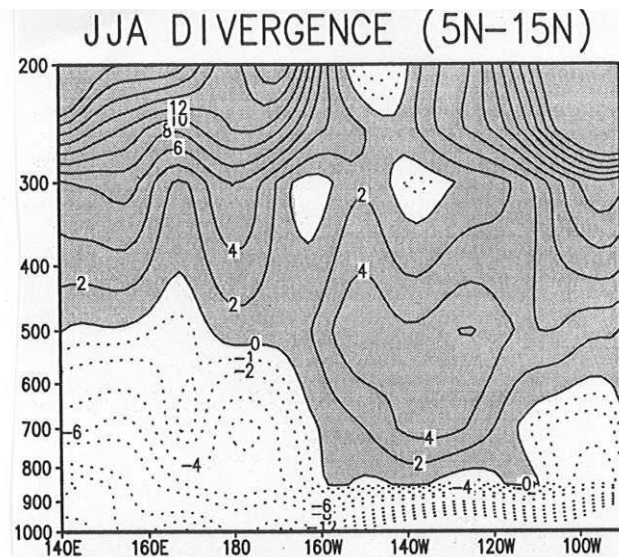
Figure 2.8b Longitude-height section of divergence for June-July-August derived from the NMC global data assimilation system averaged over 5˚ - 15˚ N to represent the Pacific ITCZ region. Shaded area indicates divergence, dotted area indicates convergence, and units are 10^{-7} s^{-1} for divergence and mb for heights (Source: Janowiak et al. 1995).

calculations based on surface divergence composites indicate that at this time enhanced large scale vapor flux convergence in this area is comparable in magnitude to the enhanced precipitation. The relative importance of surface convergence to precipitation variability is strongly supported by their findings.

Results obtained by Basher and Zheng (1998), who studied precipitation patterns over the southwest Pacific region using a partial thin plate spline fitting method were similar to Taylor's (1973) and Dorman and Bourke's (1979) results. A comprehensive modelling software package (called ANUSPLINE) was used to map precipitation data for the southwest Pacific to obtain spatially realistic rainfall maps in data sparse areas between island groups, through a statistically objective method. Their maps showed the seasonal pattern of lower rainfalls in the Southern Hemisphere winter (dry) season, from May to October and higher rainfall during summer (wet) season from November to April (Figure 2.7). They stated that high rainfall months occur in April – July period, before the ITCZ makes its seasonal shift northwards in July. According to their findings, the months January, February and March have greater than 200 mm rainfall over 70% of the region, while June, July and August have the lowest. Compared with Taylor's (1973) results, Basher and Zheng (1998) have presented similar findings, but the isohyets are smoother and statistically more realistic to some extent.

Janowiak et al. (1995) examined the east Pacific ITCZ rainfall distribution using observational datasets consisting of two preciously available in situ climatologies (Jaeger 1976 & Legates and Willmott 1990) and six satellite (microwave and IR) derived rainfall products. Their data, which ranges from July 1987 to June 1990 shows relatively high rainfall in the eastern and western ends of the ITCZ consistent with the vertical distribution of divergence (Figure 2.8a and b), which implies strong rising motion and deep convection throughout the troposphere in these regions. The in situ climatologies also depict relative maxima at the flanks of the ITCZ, which shows a significant contribution of the ITCZ towards building up the peak in precipitation. During December-January-February, a local maximum in rainfall intensity is observed in the Pacific ITCZ near 140° W, while a local minimum is observed during June-July-August. Their satellite estimates and independent data (comprising of SST, divergence and ship reports) imply that rainfall intensity decreases westward from 110° W to a minimum near 140° W and then increases to the west.

2.3.4 Precipitation Variability and El Niño Southern Oscill-ation

El Niño Southern Oscillation (ENSO) refers to the periodic alteration of atmospheric and oceanic circulations in the Pacific region and it is determined by the temperature and pressure anomalies of the ocean (Philander 1990). It was realized by Bjerknes (1969) that the sea surface temperatures (SST) in the central equatorial Pacific was either above or below normal and it fluctuated irregularly. This irregularity is related to the ENSO phenomenon, where El Niño (warm phase) corresponds to periods of high temperature departures from the normal. There is increased convective activity and cloudiness over the central tropical Pacific and a reduction in the strength of the easterly trade winds. The complementary phase of El Niño is termed La Niña (cold phase), which occurs when SST is cooler than normal across the central and eastern Pacific Ocean and the trade winds are stronger across the Pacific Ocean. ENSO events are represented by an index called the Southern Oscillation Index (SOI), which is derived from values of monthly mean sea level pressure (MSLP) at Tahiti and Darwin (Figure 2.9). Consistently positive values of the SOI correspond to La Niña events while negative values represent an El Niño situation. Since
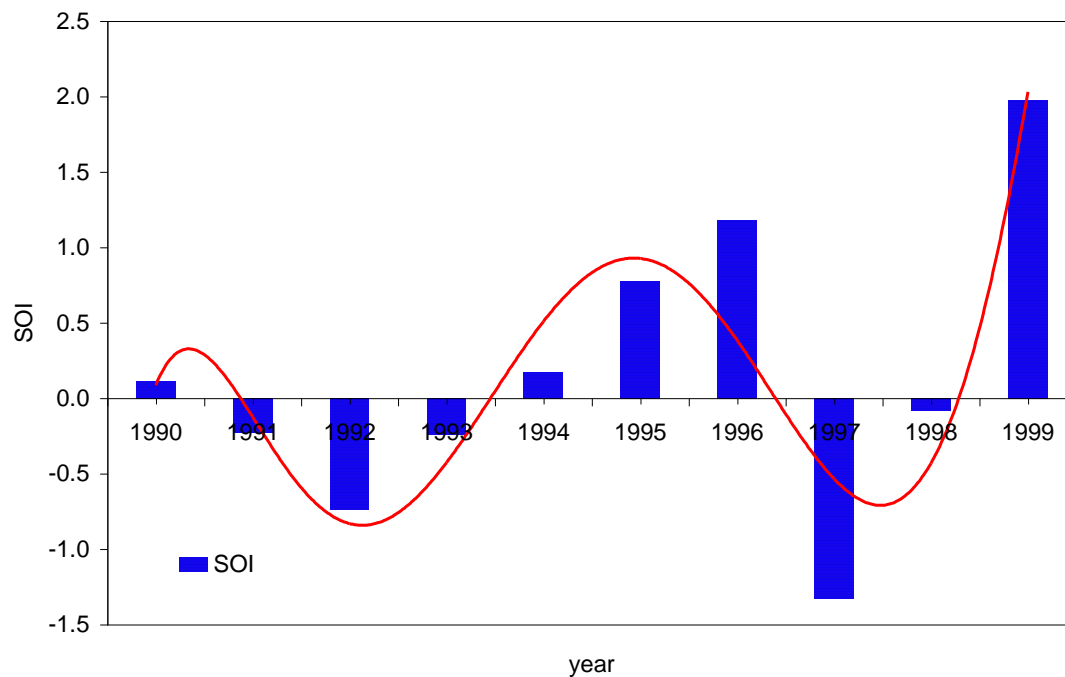
Figure 2.9   The SOI (1990-1999), illustrating the phases of the ENSO event where positive SOI corresponds to La Niña periods, while negative ones correspond to an El Niño period (data from NIWA).

19
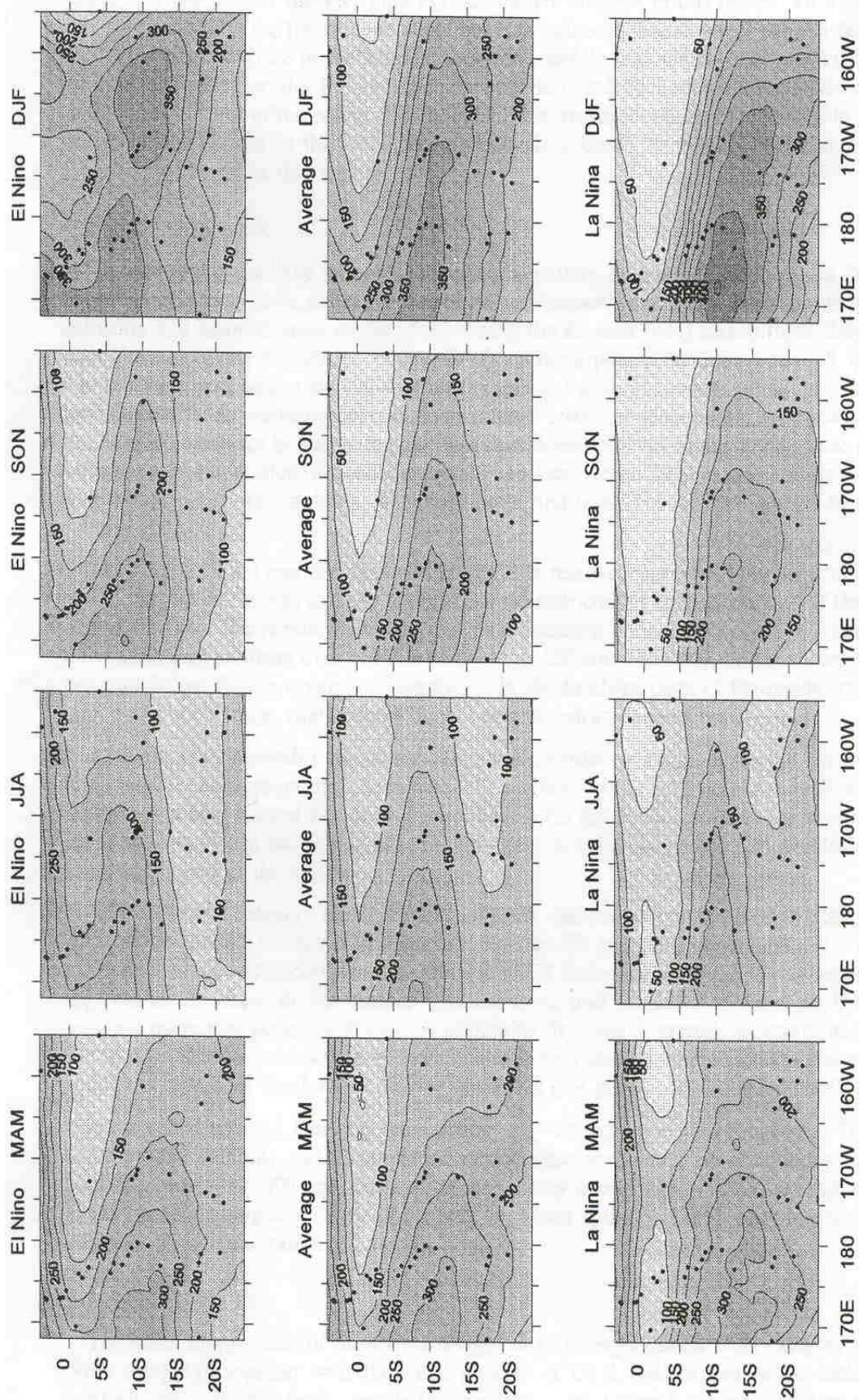
Figure 2.10   Sequence of seasonal rainfall (cm) for the southwest Pacific, for El Niño composite (top row), longterm average (middle row), and La Niña composite (bottom row), computed by partial thin-plate smoothing spline fitting method using Outgoing Longwave Radiation as the regression covariate (from Basher and Zheng 1998).
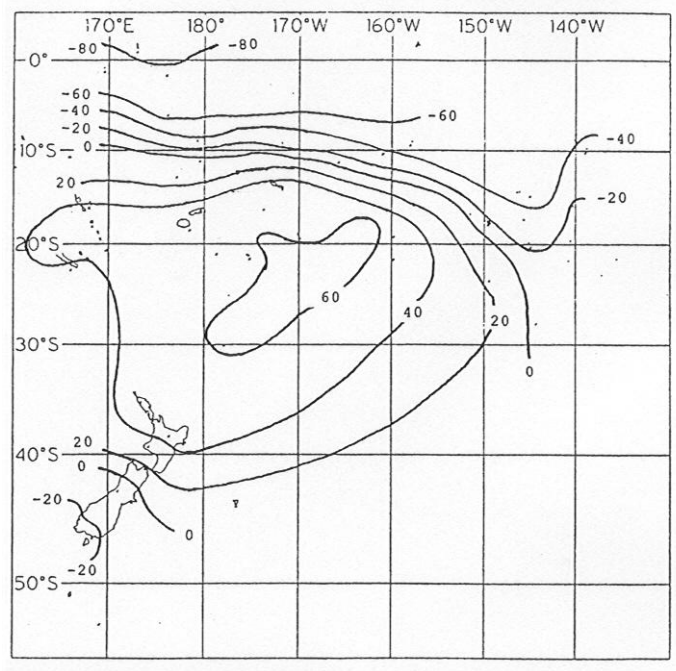
Figure 2.11   Annual correlation ($\times$ 100) between precipitation and the SOI for the southwest Pacific region. All stations with isopleths < -35 or > 35 are significant at east at the 95% level (after Salinger 1995).

ENSO is related to the changes in large-scale atmospheric circulation, precipitation variation is likely to be influenced by the alternating warm and cold phases of an ENSO event.

Rasmusson and Carpenter (1982) studied variations in tropical SST and surface wind fields associated with ENSO events. They concluded that from July to October, the most strongly developed and coherent anomaly fields are found over the western equatorial and southwest Pacific and the broad scale character of these anomaly fields seems to be associated with a southwest displacement of the SPCZ. According to Trenberth (1976), this is typical of positive SOI conditions (or below normal surface pressure and above normal SST in the central and eastern Pacific) with diminished southeast trade winds, enhanced surface circulation and precipitation in the western equatorial and western South Pacific. These conditions are significant features of a La Niña event. A seesaw in precipitation anomaly is observed to the west where below normal precipitation is observed over Indonesia during an El Niño event. Their results indicate negative precipitation anomalies associated with a weakened summer convergence zone east of Australia.

By constructing three-monthly seasonal rainfall patterns from composites of eight warm and

nine cold phases, Basher and Zheng (1998) mapped rainfall fields due to ENSO variations in the southwest Pacific region. Figure 2.10 presents the sequence of seasonal rainfall fields for the southwest Pacific for El Niño and La Niña composite computed by partial thin-plate smoothing spline fitting method with OLR (from 1976 – 1989) as the regression covariate. Contrary to La Niña, the El Niño composites exhibit more uniform rainfall fields with weaker north-south gradients and a less developed dry equatorial zone. This indicates that Hadley (north-south) circulation plays a greater role in La Niña events, while Walker (east-west) circulation plays a greater role during an El Niño event, with El Niño periods having more than five times higher rainfall than La Niña periods in the central and western Pacific. The El Niño composites demonstrate that the ITCZ extends further south, while the SPCZ shifts northwards by about 2˚ of latitude, resulting in the disappearance of the dry equatorial zone during the summer period. However, the 200 mm isohyet shifts eastward by nearly 3000 km. On the other hand, the ITCZ moves northwards and the SPCZ moves southwards by 2˚ during La Niña composites, enlarging the dry equatorial zone with the 50 mm isohyet shifting westward by nearly 3000 km. They concluded that long-term data such those that can be used to derive divergence fields can also be used to provide a better understanding of the precipitation patterns and their ENSO variations in the southwest Pacific.

Salinger at al. (1995) and Salinger at al. (1996) have documented climate trends in the southwest Pacific region, in particular studying temperature and precipitation patterns using homogenized historical climate datasets. Annual correlations between precipitation and SOI (Figure 2.11) were derived using cluster analysis as described in Willmott (1978). The figure illustrates that the SOI explains over 40 % of the year-to-year precipitation variability in the northern and central portion of the SPCZ. To the northeast of the SPCZ, correlation coefficients are increasingly negative, indicating a decrease in precipitation during La Niña conditions, while to the southeast coefficients are increasingly positive, indicating rise in precipitation during La Niña conditions. The reverse relationship is expected for El Niño events. They reported that the Southern Oscillation throughout the Oceania closely drives the inter-annual variability in temperature and precipitation.

Despite considerable research being done on ENSO related precipitation variability, there is still scope for more in-depth analysis of precipitation patterns and the impacts of El Niño and La Niña events. Different analysis techniques can be utilized to gain better understanding of the unique nature of precipitation variability due to numerous interrelated

atmospheric processes that govern ENSO events. However, there are limitations to the results of the research, depending on the approach taken and the type of data used.

Chapter 3

Data Analysis and Results

3.1 Precipitation Analysis

3.1.1 Description of Precipitation Data

Precipitation data for the tropical Pacific region (120° E – 120° W and 20° N – 35° S) was obtained from the Environment Verification and Analysis Center (EVAC) located at University of Oklahoma. Funding for the development of comprehensive Pacific Rainfall Database (PACRAIN) was provided by a research grant from National Oceanic and Atmospheric Administration (NOAA), while being jointly funded by NOAA/NASA Enhanced Data Set activity. It is managed by the Climate Change Data and Detection Program (CCDDP). The PACRAIN database consists of daily and monthly rainfall records for many sites on atolls and islands located in the South Pacific region from the period covering 1971 to 2000. This database is supplemented by an extensive collection of rainfall data from schools across the Pacific as part of the School of Pacific Rainfall Climate Experiment (SPARCE) program. A number of research organizations such as the National Institute of Water and Atmospheric Research (NIWA, New Zealand), National Climate Center (NCC, USA) and French Polynesian Meteorological Station (Tahiti) have also contributed towards developing this database. The overall management and quality assurance monitoring is provided by EVAC.

As the current research is focused on the southwest Pacific region (bounded by 155° E – 135° W and 15° N – 30° S), a subset of 53 stations was extracted from the PACRAIN database. Table 1.1 lists the altitude of each station along with a brief description of the island. Their location within the southwest Pacific region is illustrated in Figure 3.1. It

should be emphasized that most of the stations are located in the western portion of the region and south of the equator. Data in the far northeastern portion of the study region is notably quite sparse.

3.1.2 Analysis Techniques

Spatial and temporal analysis of the rainfall data was performed for the ten-year period covering 1990-1999. Since the distribution of the stations is irregular over the study region (Figure 3.1), consideration was necessarily given to the question of interpolation of data in regions where data are sparse. There was also the problem of missing data at some stations in the region.

Group	Station Name	Island Type	Altitude (m)
Fiji	Rotuma	Small, slightly hilly	26
	Nadi	Coastal and High	19
	Nausori	Coastal and high	7
	Ono-I-Lau	Small and Low	28
Cook Islands	Palmerston	Atoll	3
	Aitutaki	Atoll, slightly hilly	5
	Mauke	Small and raised	9
	Rarotonga	Volcanic and High	7
	Mangaia	Small and hilly	10
	Penerhyn	Atoll	1
	Rakahanga	Atoll	3
	Pukapuka	Atoll	3
Tonga	Niuatoputapu	Small and low hills	N / A
	Vava'u	Raised Atoll	9
	Ha'apai	Raised Atoll	2
	Nuku'alofa	Large and raised Atoll	2
Tuvalu	Nanumea	Atoll	2
	Niutao	Atoll	3

	Niu Island	Atoll	2
	Nukufetau	Atoll	2
	Funafuti	Atoll	1
	Nakulaelae	Atoll	0
	Nuilakita	Atoll	2.5
Western Kiribati	Makin	Atoll	3
	Butaritari	Atoll	2
	Tarawa	Atoll	3
	Maiana	Atoll	3
	Abemama	Atoll	3
	Beru	Atoll	2
	Onotoa	Atoll	N / A
	Arorae	Atoll	7
Eastern Kiribati	Fanning	Atoll	4
	Kirimati	Large Atoll	N / A
	Malden	Atoll	2
Tokelau	Atafu	Atoll	3
	Nukunonu	Atoll	3
	Fakaofo	Atoll	3
Solomon Islands	Auki	Rugged and elevated	11
	Honiara	Sheltered and Hilly	55
	Kira Kira	Rugged and elevated	3
	Lata	Small and Hilly	N / A
	Vanikoro	Small and elevated	N / A
French Polynesia	Atuona	Volcanic and elevated	51
	Bora Bora	Small and elevated	3
	Tahiti	Atoll	2.5
	Takaroa	Atoll	3
	Rapa	Small and hilly	2
Vanuatu	Port Vila	Some hills	N / A
New Caledonia	Koumac	Coastal, large and High	18
	Noumea	Coastal, large and High	69

| Nauru | Nauru | Raised atoll | 6 |
| Niue | Alofi | Raised atoll | 2 |

Table 3.1   Names of stations that lie in the southwest Pacific region, their island types, island groups and altitudes above sea level (taken from the catalogue of the World Meteorological Organization 2001).
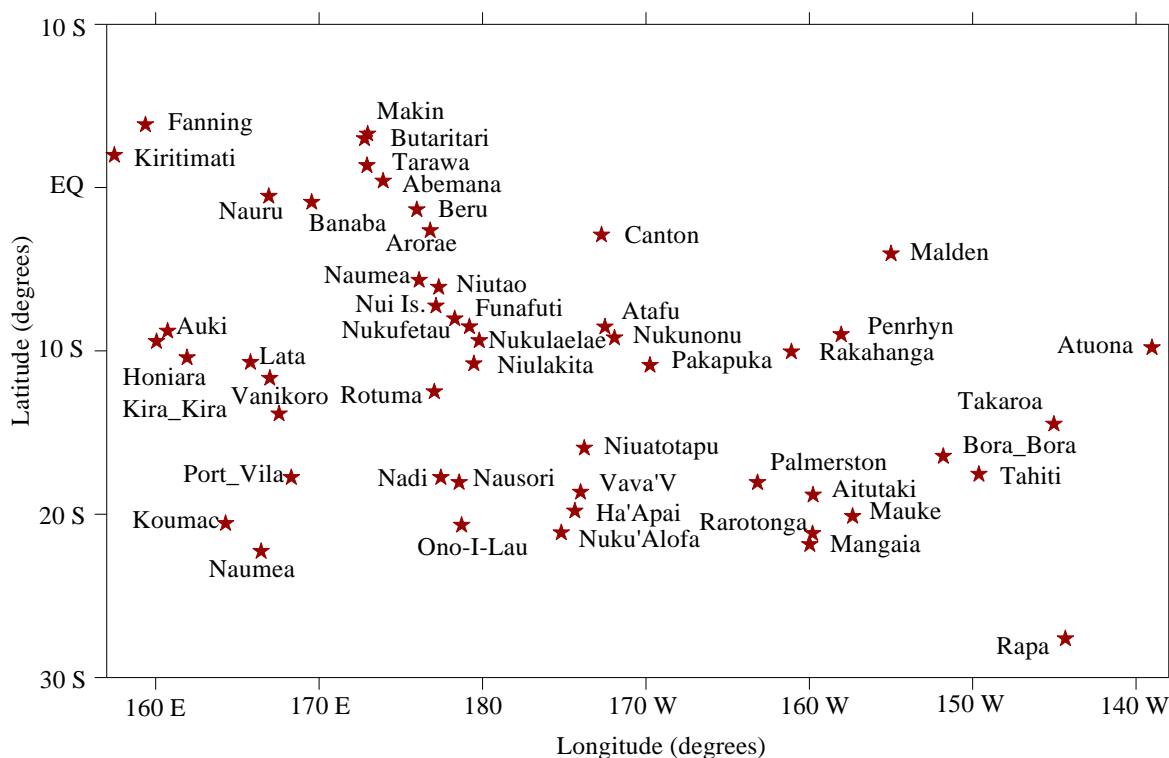
Figure 3.1   Location of rainfall stations in the southwest Pacific region. Stations are marked with stars (*).

First, the monthly rain data for the ten-year period (1990-1999) for each station was averaged to derive the mean monthly values of precipitation. Using these mean monthly values, seasonal values were computed by again averaging over the summer (December-January-February), autumn (March-April-May), winter (June-July-August) and spring (September-October-November).

To present an overall spatial pattern for the monthly and seasonal time-scales, data was interpolated to a regular grid format that had equally spaced points separated by 1.875˚

27

longitude × 1.875° latitude. Having done the regular interpolations, the problem of missing data was taken care of since it "fills" in the gaps between stations. Many methods of gridding irregular data are outlined in Keckler (1994), with different methods being better suited to different types of data, depending on dataset size and the range of values. To convert the irregular rainfall data to a suitable gridded format, the *kriging* method was used. Keckler (1994) suggests kriging as the most suitable method for datasets that are relatively small (< 250 observations) and sparse. Since the size of the dataset in the current study is relatively small (53 stations), this method was adapted to interpolate rainfall data over the southwest Pacific region of study. Kriging is a geostatistical method that attempts to express trends, which are suggested in the data, and produces a regularly spaced array of Z or rainfall values from irregularly spaced XYZ or longitude, latitude, rainfall data.

The gridded data was then run through a spline smoothing technique to improve the overall presentation. A cubical spline interpolation scheme was used to compute new grid nodes and a flexible strip (or spline) was used to draw a smooth curve between adjacent data points. This method preserves the regular grid nodes and new grid nodes are defined in order to create a surface as smooth as possible. The resulting precipitation contours (or isohyets) for the monthly and the seasonally smoothed gridded data were constructed and are presented in the following sections.

3.1.3   Monthly Precipitation Variability

Illustrated in Figure 3.2 a, b and c are the ten-year mean monthly precipitation fields for the southwest Pacific study region. Since precipitation values range from 30 mm – 450 mm per month, the median (200 mm) is highlighted in order to illustrate the changes in precipitation pattern.

Precipitation values greater than 200 mm per month cover the largest portion of the study region during January. With a progression from January to May, the area encompassed by the 200 mm decreases and continues to decrease from June to September. The smallest portion that receives greater than 200 mm per month precipitation occurs during September. The last three months of the year (October, November and December) see a gradual increase in the area receiving precipitation greater than 200 mm per month, with a continued increase till January.
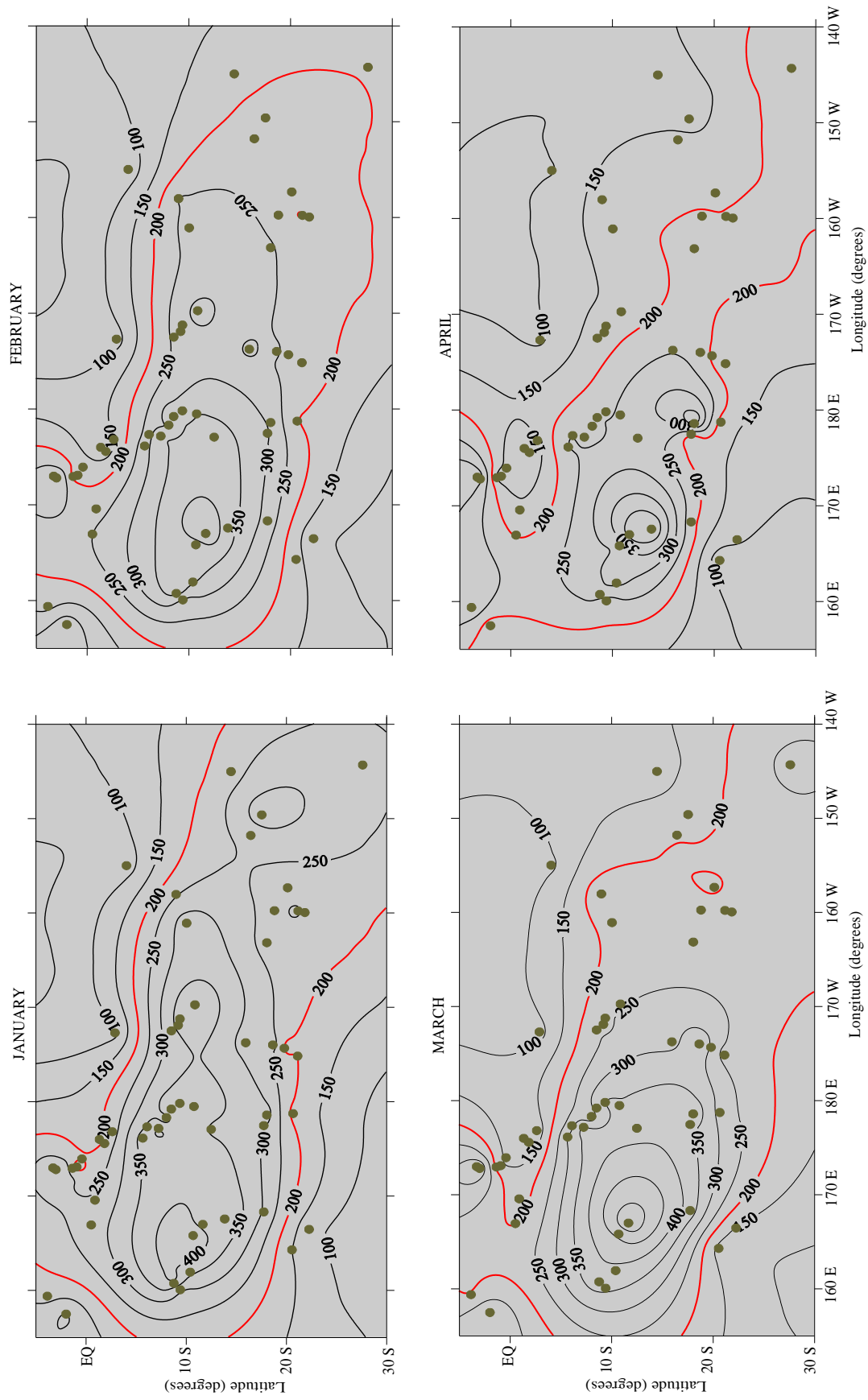
Figure 3.2a Mean precipitation (cm) during January, February, March and April averaged from 1990 – 1999 for the southwest Pacific region. Station locations are denoted as dots. The red contour line marks the 200 mm rainfall area.

There is an identifiable local maxima at around 10˚ S during all months. Two stations that are located quite close to each other and lie within the vicinity of the maximum are *Lata* and *Vanikoro* (located 10˚42' S, 165˚48' E & 11˚40' S, 166˚ 59' E respectively). These stations belong to the Solomon Islands group (Figure 3.1). Between the two stations, *Vanikoro* shows the highest precipitation throughout the year. The range of values of precipitation at this station differs through the year with a maximum value of 563 mm per month during September and a minimum value of 353 mm per month during November.

The horizontal spread of the isohyets undergoes a significant change from January to December as seen in Figures 3.2a, b, and c. The 200 mm isohyet covers a much larger horizontal extent during the month of January when compared with other months. For example, it covers the entire horizontal (east-west) region during January but during May, it covers only the region from 160˚ E - 175˚ W. During June, it is few degrees larger than May. However, during July and August, the horizontal extent of the 200 mm isohyet remains almost the same, while it is the smallest during September, covering between 160˚ E – 180˚. From September to December, the shape and size of the horizontal portion changes back to what it was during January. It is clear that the central western end of the region shows enhanced precipitation while the northeastern end has reduced rain.

It is observed that stations that are located in the western portion of the southwest Pacific region will receive higher rain than those in the eastern portion. Referring to Figure 3.1, the stations located in the islands groups of French Polynesia experience lower rainfall than Vanuatu, Solomon Islands, New Caledonia and Fiji.

Since the months of January and July are the considered to be the wettest and driest months of the year respectively for the islands located in the southwest Pacific region (Dorman and Bourke 1979 & Basher and Zheng 1998), it is important to examine the precipitation patterns more closely during these months. Consider the precipitation patterns during January and July from Figure 3.2. The key feature of the precipitation patterns during the two months is the local maximum at around 10˚ S, the structure and spatial extent of the 200 mm isohyet lines and the sub-region of minimum precipitation in the northeastern corner of the region.
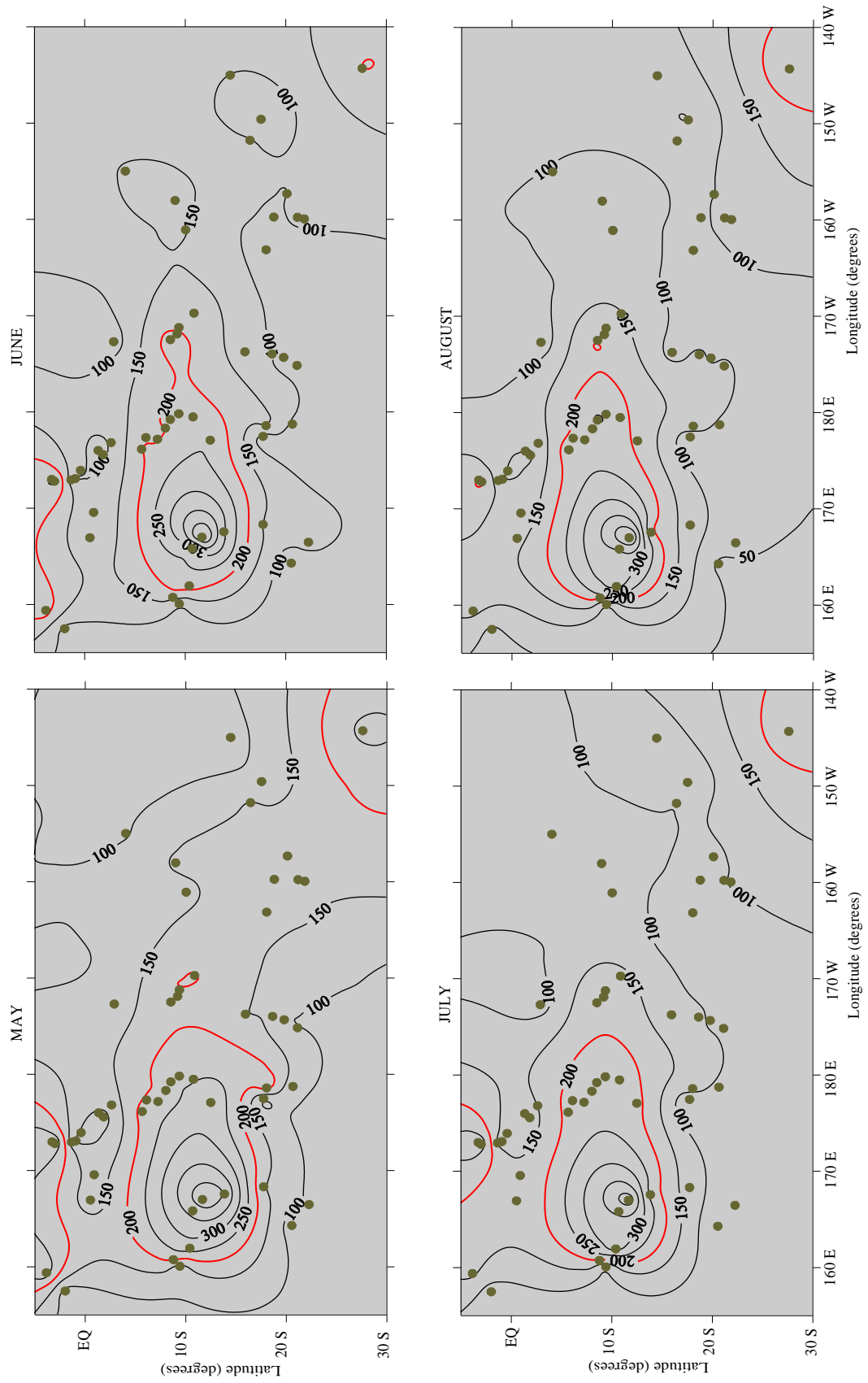
Figure 3.2b Mean precipitation (cm) during May, June, July and August averaged from 1990 − 1999 for the southwest Pacific region. Station locations are denoted as dots. The red contour line marks the 200 mm rainfall area.
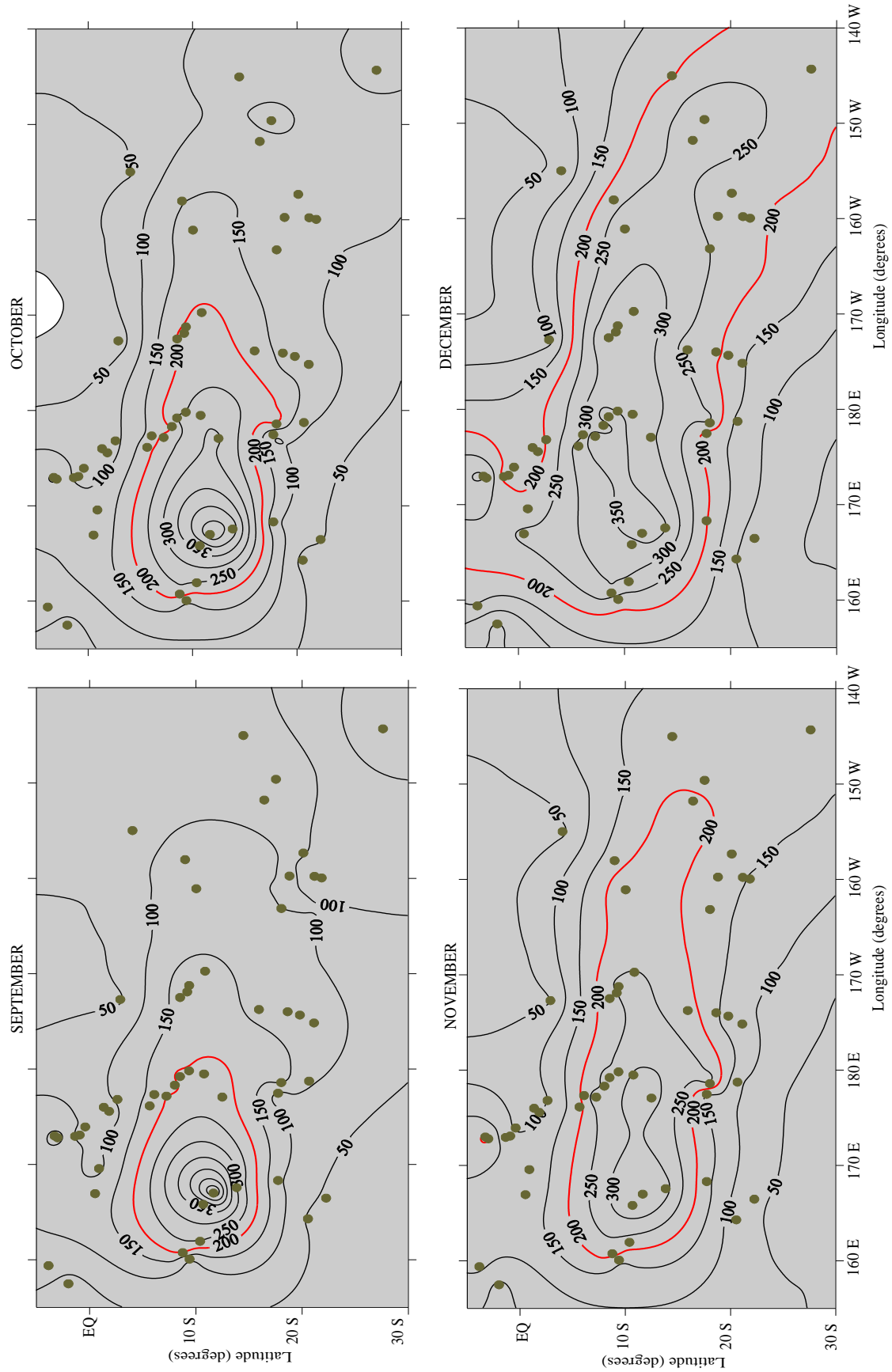
Figure 3.2c Mean precipitation (cm) during September, October, November and December averaged from 1990 – 1999 for the southwest Pacific region. Station locations are denoted as dots. The red contour line marks the 200 mm rainfall area.

The local maximum, which occurs at the stations *Lata,* has a value of 416 mm per month during January and 381 mm per month during July respectively. The spread of 200 mm isohyet is greatly reduced since it covers a relatively smaller space in the southwest Pacific region during July. To the far northeastern end of the region (160˚ W - 140˚ W and north of the equator), lower precipitation isohyets of 50 mm can be noted during January, while higher precipitation (100 – 150 mm) is evident during July. On the whole, a majority of stations, which are located in the western end of the region experience reduced rain while those on the northeastern end experience an increase in the amount of rainfall.

3.1.4   Seasonal Precipitation Variability

Illustrated in Figure 3.3 and Figure 3.4 is the precipitation pattern for summer, autumn, winter and spring. The long-term rainfall trends show distinct features during each season. Two such features are the rise and fall in rain during the seasonal change in the northern and southern portion of the southwest Pacific region. In the northwestern part, highest precipitation occurs during the autumn, decreasing in winter and spring followed by an increase in summer. However, the trend is different for the southern portion. Maximum precipitation occurs during summer and minimum during spring, while winter and autumn are intermediate seasons.

Further observation of the broad precipitation pattern shows a change in the structure of the isohyets at the equator. Here, the isohyets in northern and southern hemispheres are separated by a boundary of a local minimum, which occurs around the equator. Further to the north and south of the equator, the value of the isohyets increases. In the Southern Hemisphere, it maximizes at approximately 10˚ S. One major island group, which lies on the equatorial belt that would receive low rainfall, is the Western Kiribati (Table 3.1 and Figure 3.1).

Other interesting precipitation features that were present in the monthly patterns are naturally visible in seasonal plots as well. The 200 mm isohyet starts from the western side of the region, passing through the central part and ending on the southeastern side of the study region during summer, but during autumn, winter and spring, it is located in the western portion of the region only. While the precipitation in summer is similar to that in autumn, precipitation in winter is similar to spring.
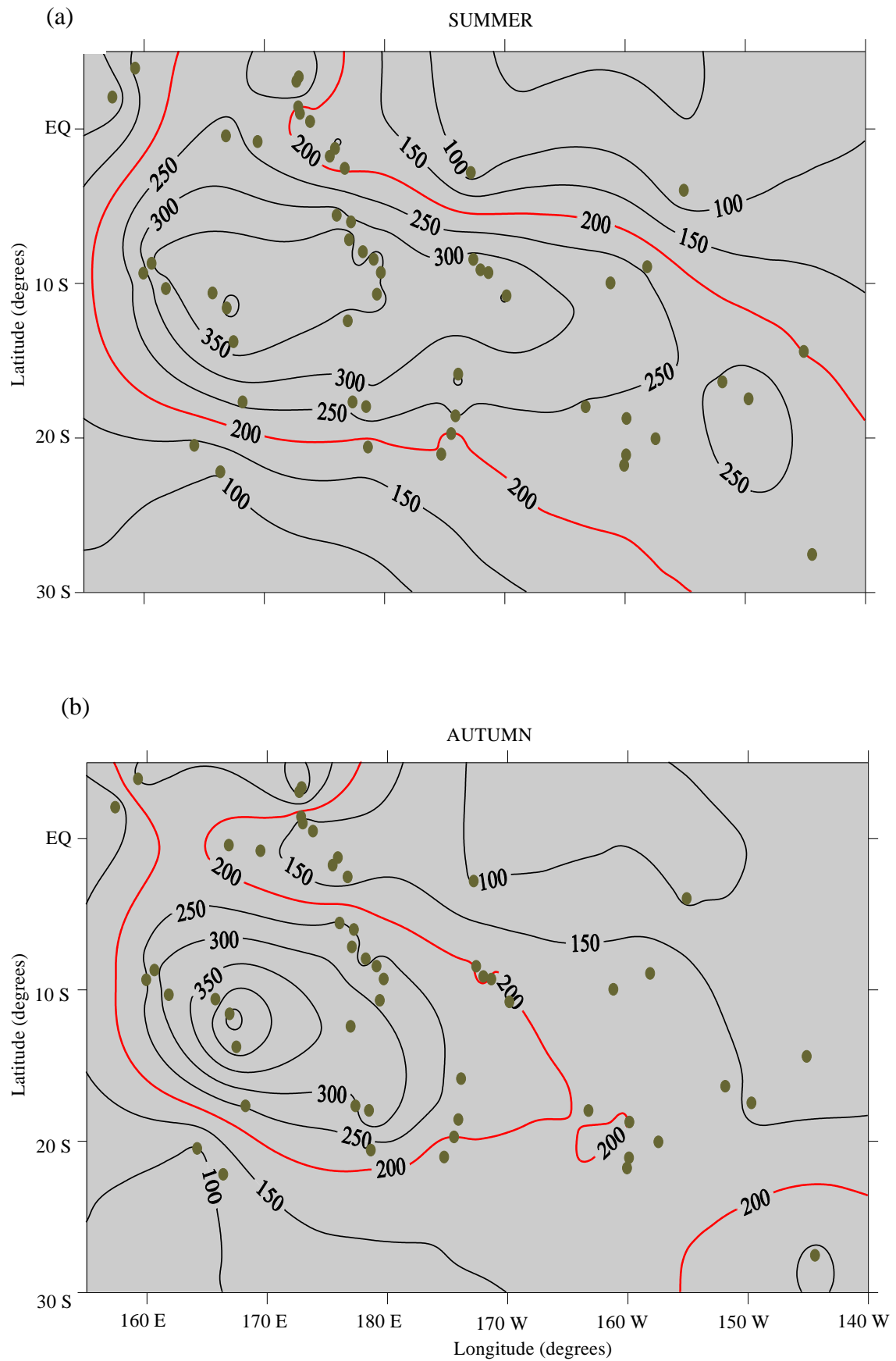
Figure 3.3   Monthly averages of seasonal precipitation patterns for the southwest Pacific region for (a) Summer [Dec-Jan-Feb] (b) Bottom: Autumn [Mar-Apr-May].

(a)

WINTER

(b)
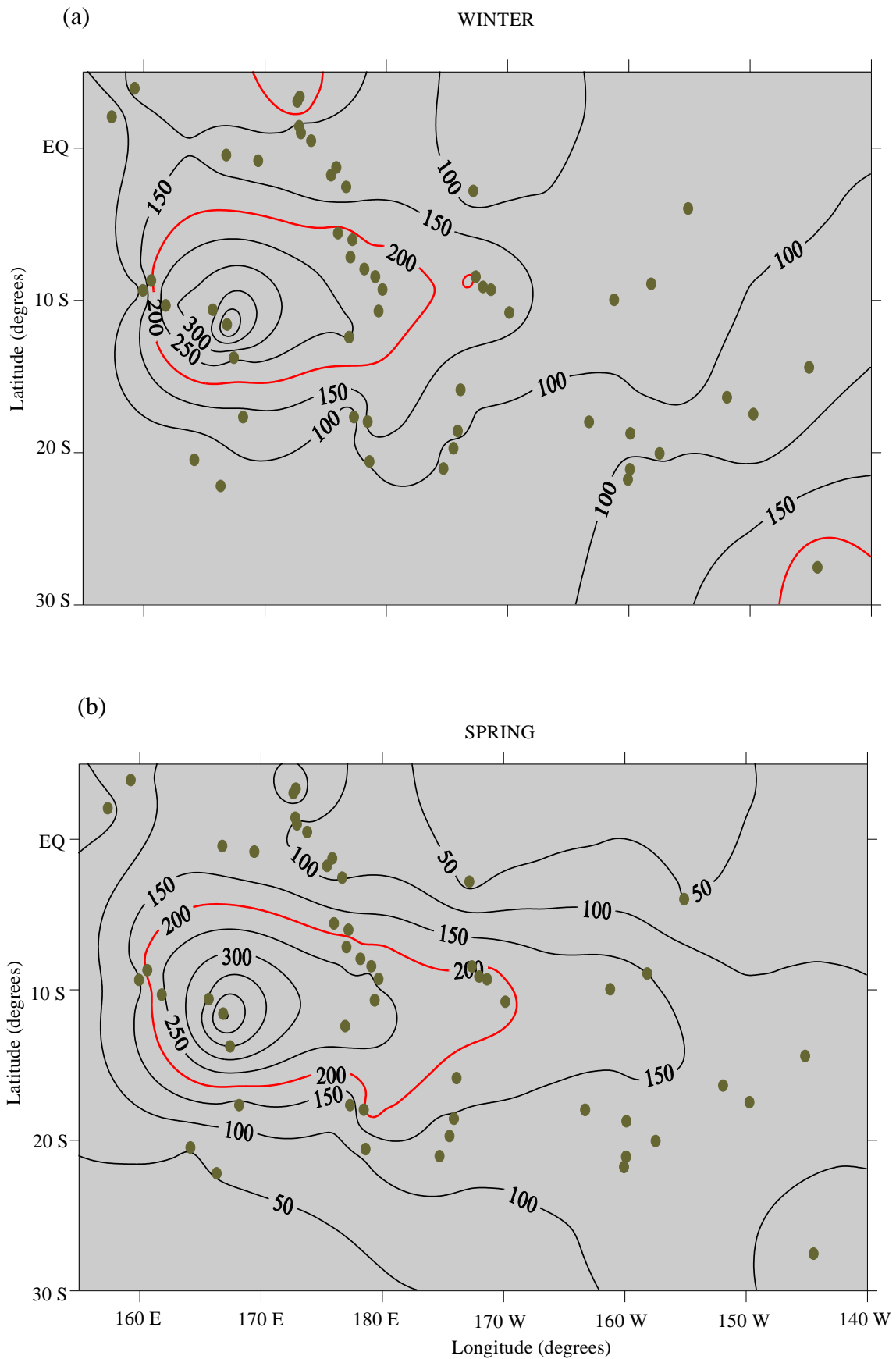
SPRING

Figure 3.4 Monthly averages of seasonal precipitation patterns over the southwest Pacific region for (a) Winter [Jun-Jul-Aug] (b) Spring [Sept-Oct-Nov].

3.2   Airflow Patterns

3.2.1   The Reanalysis Wind Data

The National Center for Environment Prediction/National Center for Atmospheric Research (NCEP/NCAR) reanalysis data, which is described in Kalnay et al. (1996), was obtained from the National Institute of Water and Atmospheric Research (NIWA), New Zealand. The NCEP/NCAR Reanalysis Project is a joint project between the National Centers for Environmental Prediction (NCEP, formerly "NMC") and the National Center for Atmospheric Research (NCAR). The goal of this joint effort is to produce new atmospheric analyses using historical data (1948 onwards) and also to produce analyses of the current atmospheric state (Climate Data Assimilation System, CDAS). This principal dataset comprised of zonal and meridional winds at the surface (10 m above sea level) and at the 200-hPa level. The reanalysis data extracted was composed of daily observations of zonal and meridional winds from 1990 – 1999.

This dataset was constructed using data obtained from radiosonde, satellite, aircraft, shipping measurements and from the meteorological station observations. Global climatological datasets that were previously available, such as the Comprehensive Ocean-Atmosphere Datasets (COADS) have also been incorporated into these records. Reanalysis of the combined dataset was performed using an operational spectral forecast model with T62 resolution (28 vertical levels and grid resolution of approximately 210 km). Kalnay et al. (1996) stated that the analysis cycle, with the use of a 6-hr forecast as a first guess is able to transport information from data rich to data poor regions so that even in data void areas, the reanalysis can estimate the evolution of the atmosphere over synoptic and climatological scales. Inaccurate data, which might cause problems for the model, are eliminated from the analysis by the assimilation scheme. Model outputs are subject to an automated quality control check for every six hour forecast period. Furthermore, comparisons between the reanalysis output and real observations are done, and it shows that the deviations between them are very small.

The surface data has a grid resolution of 1.875˚ × 1.875˚, running from 90˚ N – 90˚ S and 0 – 360˚. Data at 200 hPa has a grid resolution of 2.5˚ × 2.5˚. From this global dataset, gridded surface and 200-hPa wind data for the western Pacific region (bounded by
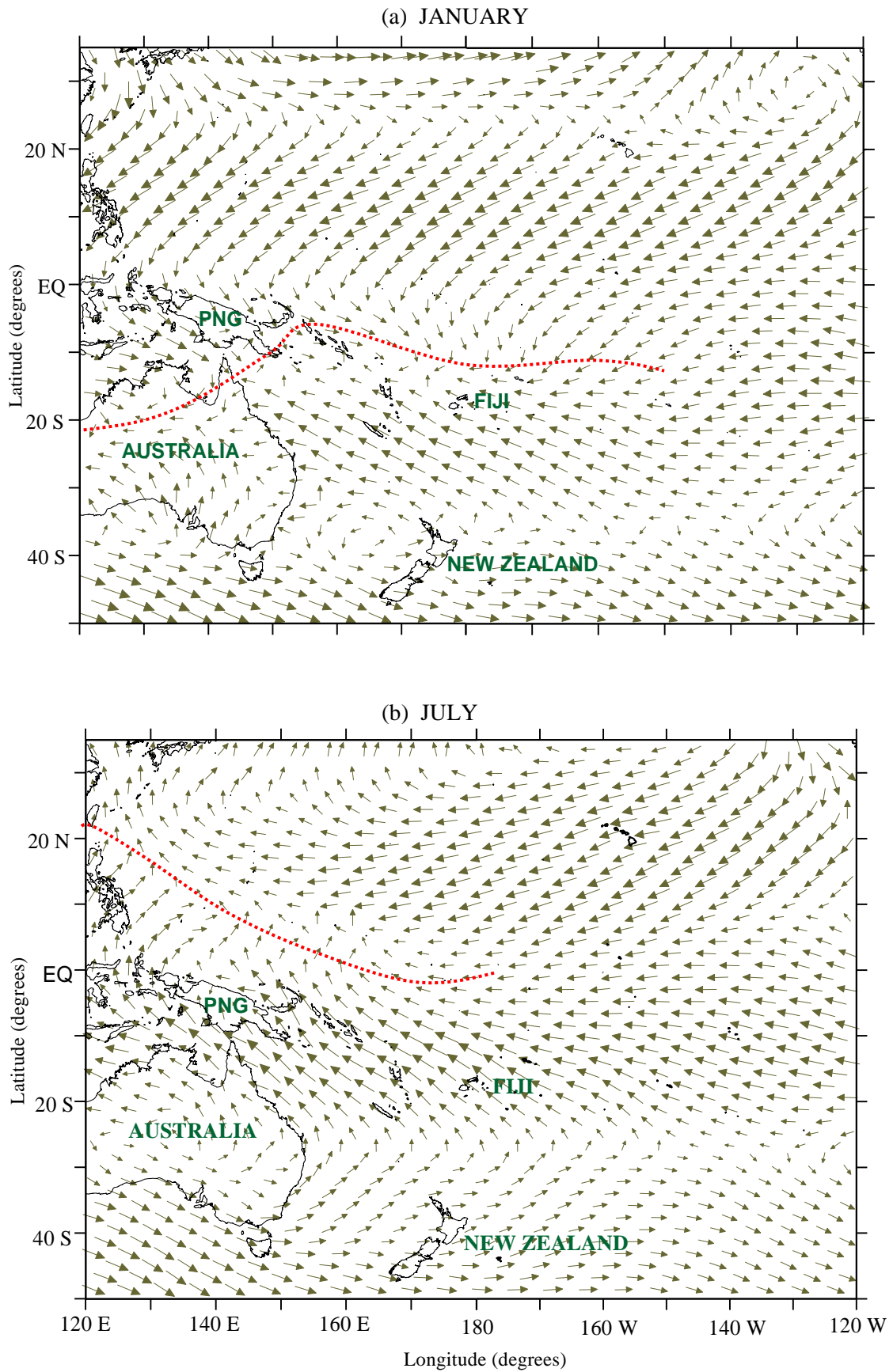
Figure 3.5 Mean resultant surface wind field (1990 – 1999) for the western Pacific region for (a) January and (b) July. The red line indicates the boundary of convergence during the two months.

120˚ E – 120˚ W and 35˚ N – 50˚ S) is extracted even though the region of precipitation study is the smaller southwest Pacific region (bounded by 155˚ E – 135˚ W and 15˚ N – 30˚ S). To explain the precipitation variability in this area, one needs to understand the dynamical processes inside, as well as outside the southwest Pacific region. Thus, a larger region is selected for the wind analysis and the sub-region for precipitation study lies within this larger region.

3.2.2   Surface Airflow Patterns

Using the surface wind speeds and directions at the regular grid spacing of $1.875˚ \times 1.875˚$, the ten-year monthly wind field is plotted for the months of January and July, as well as the seasonal average patterns. Figure 3.5 illustrates the ten-year (1990 – 1999) mean surface airflow regime for the months of January and July for the western Pacific region.

The dominant features include the trade wind belts in the Northern and Southern Hemispheres and the boundary of convergence (highlighted in the dotted red line) between the northeast and southeast trade winds. In the Northern Hemisphere, the northeast trades extend westward into the North Pacific. These winds, however, are stronger than the southeast trade winds in the Southern Hemisphere. The July wind field in the Northern Hemisphere is stronger in the eastern and weaker in the western side of the region. Some anti-cyclonic flow is noted around 20˚ N of the equator, on the far western side. The July wind field shows that the southeast trades cover the horizontal (east-west) section of the western Pacific from about 5 – 15˚ S, while during January, they are located from 15 – 35˚ S in the Southern Hemisphere.

The dotted red line shows the boundary of convergence on the surface wind plots. Associated with this region is a weak wind flow (low magnitude vectors) and the approximate position of the ITCZ. The northeast and southeast trade winds meet at this boundary. The ITCZ is located below the equator during January; it is associated with wind speed minimum and convergence in the surface winds. The SPCZ, though not quite conspicuous, can be depicted roughly to be located diagonally from northeastern PNG to Fiji and is merged with the ITCZ at the equator. However, during July, the ITCZ has shifted northwards by at least 6 – 8˚.
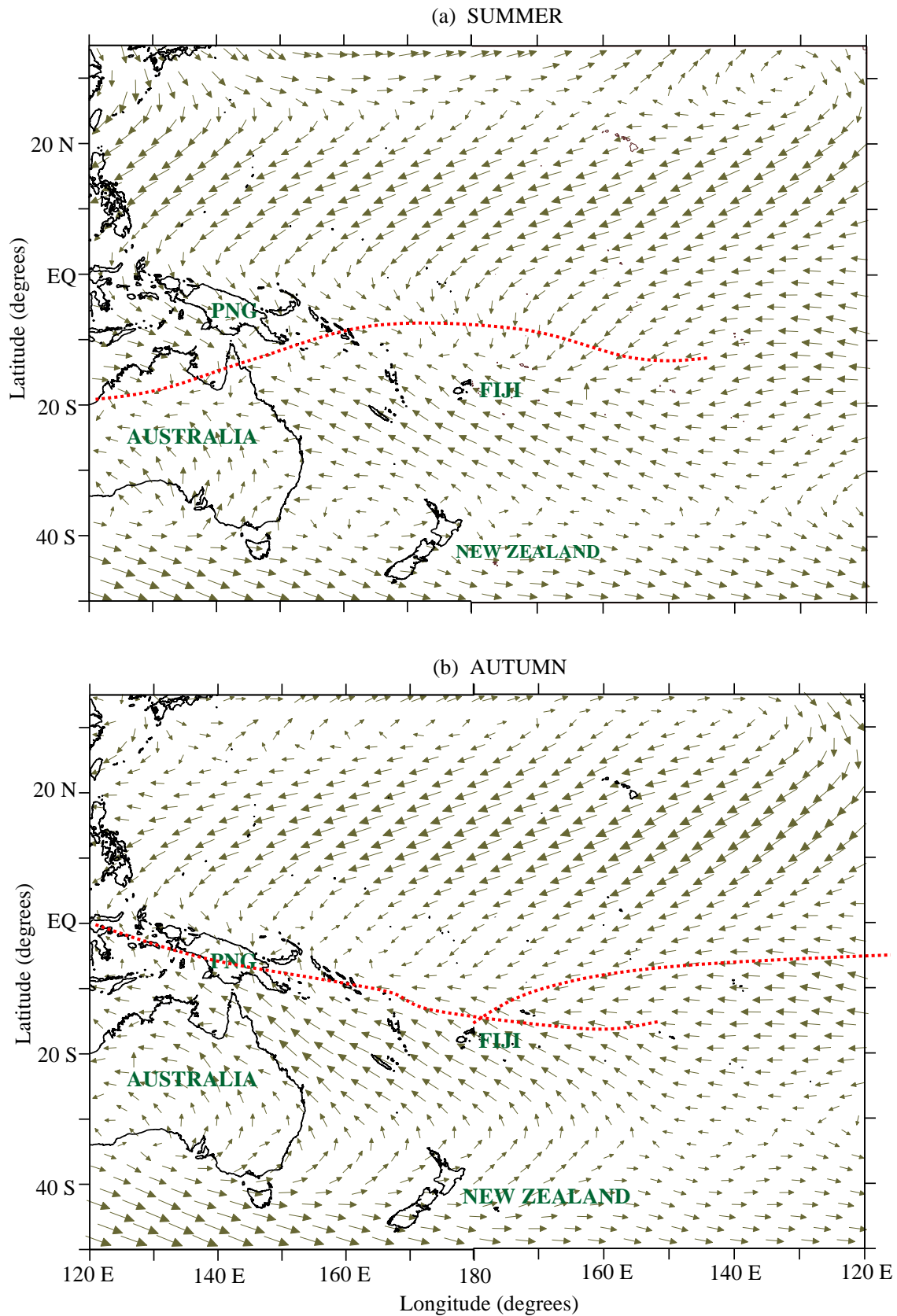
Figure 3.6 Mean surface resultant surface wind field (1990 – 1999) for the western Pacific region for (a) summer and (b) autumn. The red line indicates the boundary of convergence during the two months.
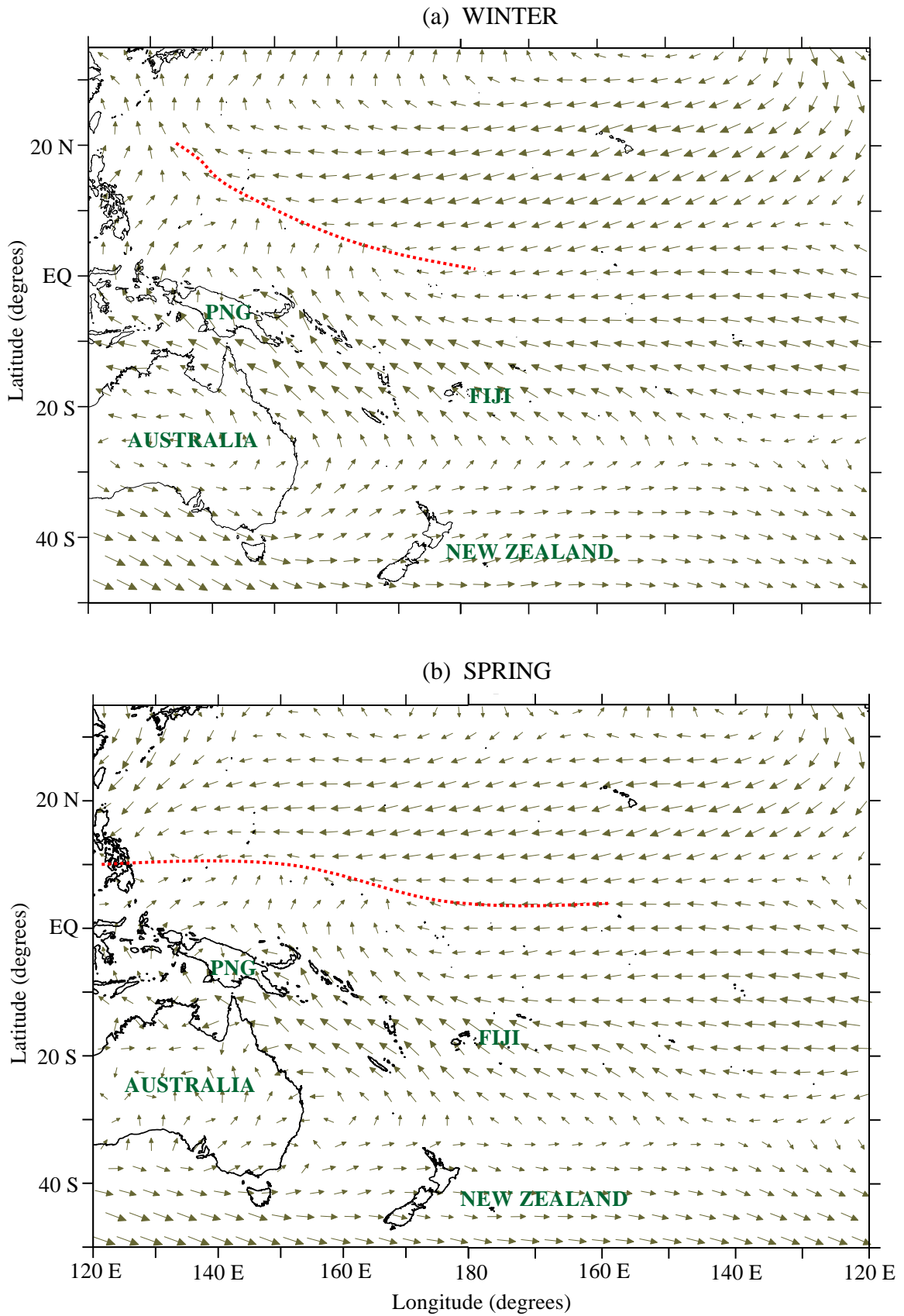
Figure 3.7   Mean resultant surface wind field (1990-1999) for the western Pacific region for winter and spring. The red line indicates the boundary of convergence during the two months.

westward horizontal shift. Figure 3.6 and Figure 3.7 present the seasonal patterns of the mean surface wind field. In summer, the northeast trades occupy the largest horizontal portion (120˚ E – 120˚ W) of the northern Pacific while it is reduced during autumn (130˚ E – 130˚ W). Their horizontal extent is the smallest in winter (150˚ E – 130˚ W), while increases again in spring (145˚ E – 125˚ W). This shows the seasonal variability of the horizontal extent of the trade winds in the Northern Hemisphere. On the other hand, the southeast trades are located from 145˚ E – 135˚ W in summer, while they are located from about 135˚ E – 130˚ W in autumn. These positions show the westward shift of the winds from the summer to autumn. In winter and spring, they are located at almost the same positions as autumn although slightly further north. Compared with the northeast trades, the southeast trades cover a relatively smaller horizontal portion of the region during all seasons.

Marked in red dotted lines are the seasonal positions of the convergence zones. The ITCZ is located furthest north in winter (at about 10˚ N) and furthest south in summer. It is shown that the SPCZ (not quite conspicuous) is located diagonally and merged into the ITCZ during all the seasons. In spring, the convergence zone is the weakest and least conspicuous. Another significant feature is the westerly flow at latitudes greater than 40˚ S during all seasons. The direction of the flow changes from westerly to southeasterly between 30 and 40° S.

The surface wind plots demonstrate the possible positions of the convergence zones but further analysis is needed to relate precipitation variability to the position, intensity and movement of the convergence zones. The surface wind fields are used to produce images of the convergence zones using the concept of continuity as explained in the next section. The characteristics of the convergence zones will then be used to explain precipitation variability in the current study region.

3.3   Concept of Continuity and Convergence

Weather systems are referred to as three-dimensional systems that result from interactions of temperature and pressure patterns. The changing patterns of temperature and pressure are responsible for the origin, maintenance and intensification of weather systems. The concept

of continuity is often treated as one of the major ideas used to explain changing weather systems, which can be described using the idea of convergence and divergence of the resultant flow (Sturman and Tapper 1996).

In simple terms, the concept of continuity states that in order to maintain a weather system such as a depression, " the rate of inflow in the centre of the system must be balanced by an equal rate of vertical outflow to higher levels". Similarly, to intensify the system, the rate of vertical outflow must be greater than the inflow at the surface and to decay a system, it needs to be less so that air accumulates and the depression "fills". Figure 3.8 shows a simple representation of the concept of continuity, relating the inflow into and outflow from a unit volume (Sturman and Tapper 1996).
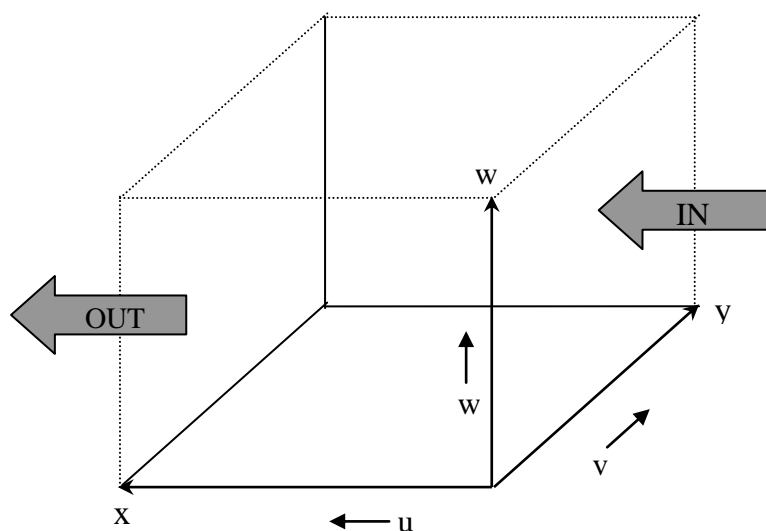
Figure 3.8   Unit volume showing the concept of continuity, taking into account the three-dimensional nature of the flow (after Sturman and Tapper 1996).

Mathematically, the continuity equation states that

$$\frac{dp}{dt} = -p\left(\frac{\partial u}{\partial x} + \frac{\partial v}{\partial y} + \frac{\partial w}{\partial z}\right)$$
[1]

where $\frac{dp}{dt}$ is the rate of change of pressure in the unit volume, u is the zonal wind speed, v is the meridional wind speed, w is the vertical wind speed and x, y and z are the components of the rectangular coordinate system. Since the density of air is related to the pressure that it

42

exerts, accumulation of air in the unit volume (or convergence of air) leads to a rise in the air pressure, while depletion of air (or divergence of air) leads to a decrease in air pressure in the unit volume. Therefore, it can be interpreted from Equation [1] that when the partial derivative $\left[\dfrac{dp}{dt}\right]$ is positive, the term $\left[\dfrac{\partial u}{\partial x}+\dfrac{\partial v}{\partial y}+\dfrac{\partial w}{\partial z}\right]$ is negative and the system is convergence. Similarly, when the rate of change of pressure is negative, the system is divergent since the term $\left[\dfrac{\partial u}{\partial x}+\dfrac{\partial v}{\partial y}+\dfrac{\partial w}{\partial z}\right]$ is positive.

In practical weather systems, vertical velocity, w is relatively small when compared with the zonal and meridional velocities (Holton 1992). Neglecting the vertical velocity, the horizontal divergence term becomes

$$div_h V = \left(\frac{\partial u}{\partial x}+\frac{\partial v}{\partial y}\right) \qquad [2]$$

where V is the velocity field. This equation can be used to estimate the accumulation or depletion of air mass over a given horizontal surface due to spatial variations in the airflow speed and direction at that level. Maps of convergence and divergence can be easily derived using gridded wind speed and direction data and finite difference approximation. Using these maps, one can estimate the vertical motion that is likely to occur between two levels in the atmosphere. As documented by Basher and Zheng (1990), the convergence and divergence zones, which assist in vertical motion in the atmosphere, are related to precipitation variability. Therefore, it is crucial that divergence fields for the surface and upper levels are considered while studying the dynamics of precipitation variability.

3.3.1   Derivation of Horizontal Divergence Fields

The gridded NCEP/NCAR reanalysis wind data are used to calculate the surface horizontal divergence fields (10 m above sea level) at regular grid spacing of 1.875˚ × 1.875˚, within the western Pacific region (120˚ E – 120˚ W, 35˚ N – 50 ˚ S).

Zonal and meridional velocity (u and v) components are obtained at grid points with a grid spacing of 1.875 ° × 1.875° as shown in Figure 3.9.
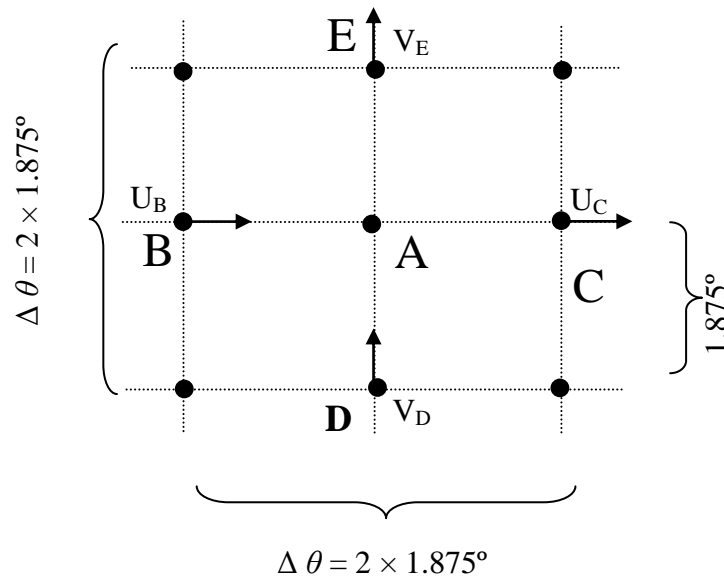
Figure 3.9   Sample grid for calculating surface horizontal divergence using zonal and meridional wind vectors.

To calculate the horizontal divergence at A, four horizontal velocity vectors at B, C, D and E are considered. Firstly, the distance between any two-grid points is calculated using the latitude and longitude of these points: Firstly, the X-spacing distance between the two grid points, B and C are given by

$$\Delta X = \frac{\pi}{180}(\Delta\theta)R\cos|\Phi| \qquad [3]$$

where ΔX is the spacing between the points B and C (in metres), θ is the change in longitude (in degrees) from B to C, R is the Earth's radius (6.637×10^{6} m) and Φ is the latitude of point A. However, to calculate the Y-spacing between two points, a slightly different expression is used, since this is dependent on the latitude and Earth's radius only.

The Y-spacing distance between the two grid points, D and E are given by

$$\Delta Y = R\Delta\Phi\left(\frac{\pi}{180}\right) \qquad [4]$$

where ΔY is the spacing between the points D and E (in metres), and other symbols are as defined for Equation [3]. Using these distances and the zonal and meridional velocities, the horizontal divergence is found using

$$Div_h U = \nabla_h . U = \frac{\partial u}{\partial x} + \frac{\partial v}{\partial y} \qquad\qquad [5.1]$$

Or in finite difference form,

$$Div_h U = \nabla_h . U \approx \frac{\Delta u}{\Delta X} + \frac{\Delta v}{\Delta Y} \qquad\qquad [5.2]$$

Using Equation [5.2], horizontal divergences at the surface (10 m above sea level) and at 200-hPa were calculated to examine the nature of flow at these levels. However, the grid spacing is $2.5° \times 2.5°$ at 200-hPa, but the method remains the same.

The horizontal divergences are then used to produce January, July and seasonal images of atmospheric convergence zones using the arguments that highly negative divergence leads to convergence and positive divergence leads to divergence of the flow as explained by the principle of continuity. The approach taken, in this study to locate the convergence zones is consistent with that taken by Zheng et al. (1997) who studied seasonal and inter-annual variability of atmospheric convergence zones over the tropical Pacific region using data from European Remote Sensing (ERS)-1 scatterometer. Furthermore, the January, July and seasonal precipitation patterns are overlaid on the horizontal divergence fields and any trends in precipitation due to the convergence and divergence of the flow are explained.

3.3.2 Surface Horizontal Divergence Fields

Figure 3.10a illustrates the mean surface horizontal divergence fields during January, calculated from averaged zonal and meridional velocities from 1990 – 1999. The plot shows large horizontal regions of negative divergence (of magnitude between -2×10^{-6} and -6×10^{-6} s^{-1}) located at about $10 – 15°$ S of the equator, and extending from $130°$ E $– 140°$ W in the horizontal (east-west) postion. This could be interpreted as the approximate position of the merged ITCZ and the SPCZ. A large portion of the central southwest Pacific region
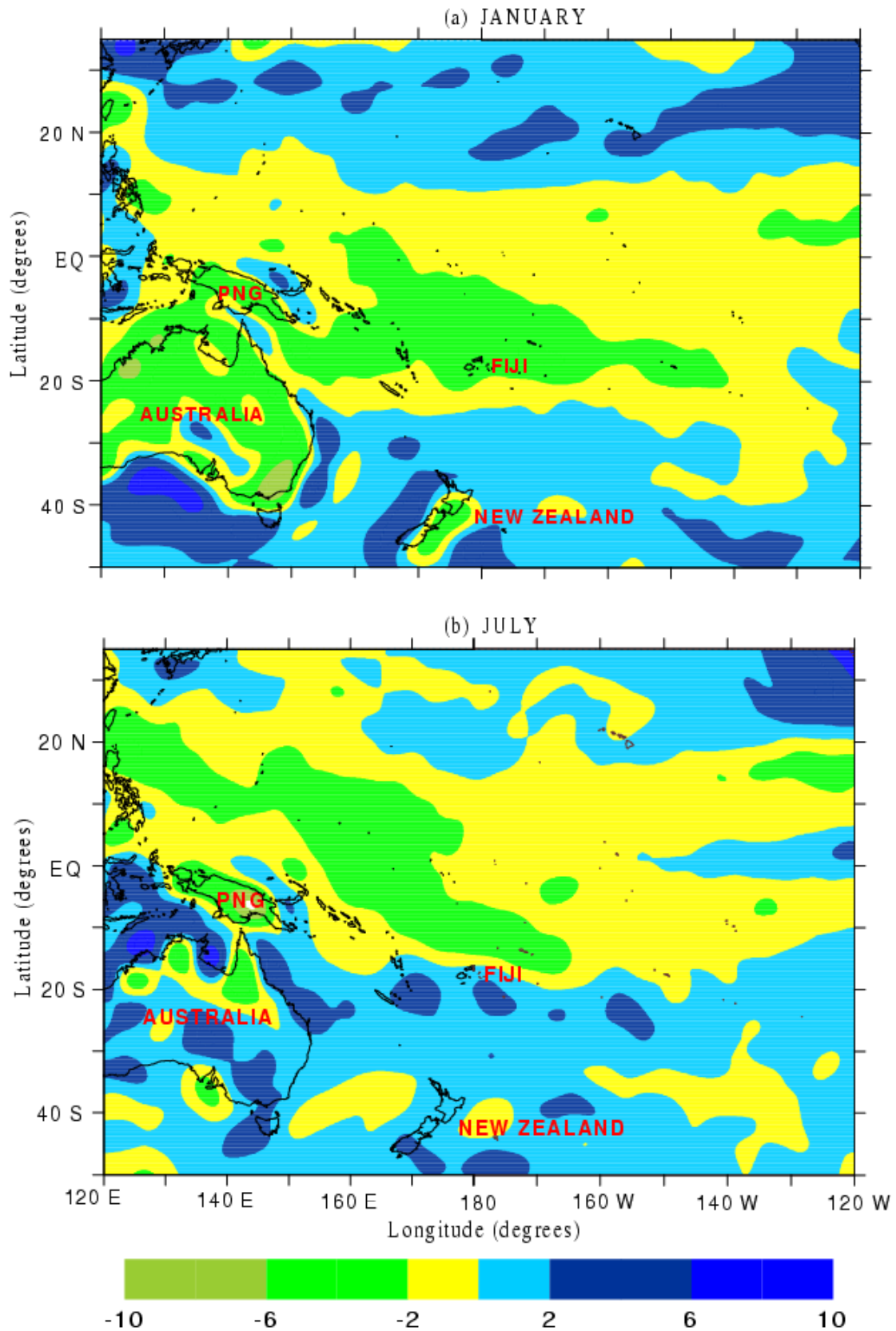
Figure 3.10   Color-coded image of mean surface horizontal divergence (1990 – 1999) ($\times$ 10^{-6} s^{-1}) for the western Pacific region during (a) January and (b) July.

46

shows convergence of surface winds, which is the usual position of the SPCZ. However, large negative divergence of this magnitude can also be noted around Australia. As it occurs in summer, it could relate to the thermal effect of the continent.

However, major emphasis of this research is on the western central Pacific region, which does not include Australia. When considering the wind plots for January, these regions of negative divergence are also visible in the form of low-magnitude and disorganized wind vectors which can be noted on the same region on Australia which have led to large negative divergence fields as seen in Figure 3.10. The region of negative divergence which has emerged diagonally from PNG to Fiji is the postion of the SPCZ, but well south of the equator, which is merged with the ITCZ when it enters the western Pacific.

Figure 3.10b also shows the mean surface horizontal divergence fields for the month of July. The region of high convergence (large negative divergence) has changed from what was seen during the month of January. The region has extended to a larger vertical position and it is located diagonally from 20° N − 20° S and extending over a relatively smaller horizontal portion in the central western Pacific. It extends further into the Northern Hemisphere during July. Associated with this is the northward movement of the divergence fields.

Figure 3.11 shows the mean horizontal divergence at 200-hPa for January and July. This is the pattern seen at the tropopause, which is located at approximately 12 km from the ground. Comparing the divergence fields at the surface and at the tropopause for both the months, one can say that low-level convergence (at the surface) leads to upper level divergence (at 200 hPa). The divergence fields also show a slight westward shift at 200 hPa. This is the striking feature of the ITCZ, which has been explained in Sturman and Tapper (1996).

Air motion charateristics at the surface and at the tropopause are shown in Figure 3.12. Air enters the column at the surface and leaves at the higher level in the atmosphere to maintain the continuity of the flow. This is clearly illustrated by the horizontal divergence fields during January and July at the surface and at 200 hPa. Convergence (negative divergence) at the surface leads to divergence (positive divergence) at the same location but at a higher level in the atmosphere.
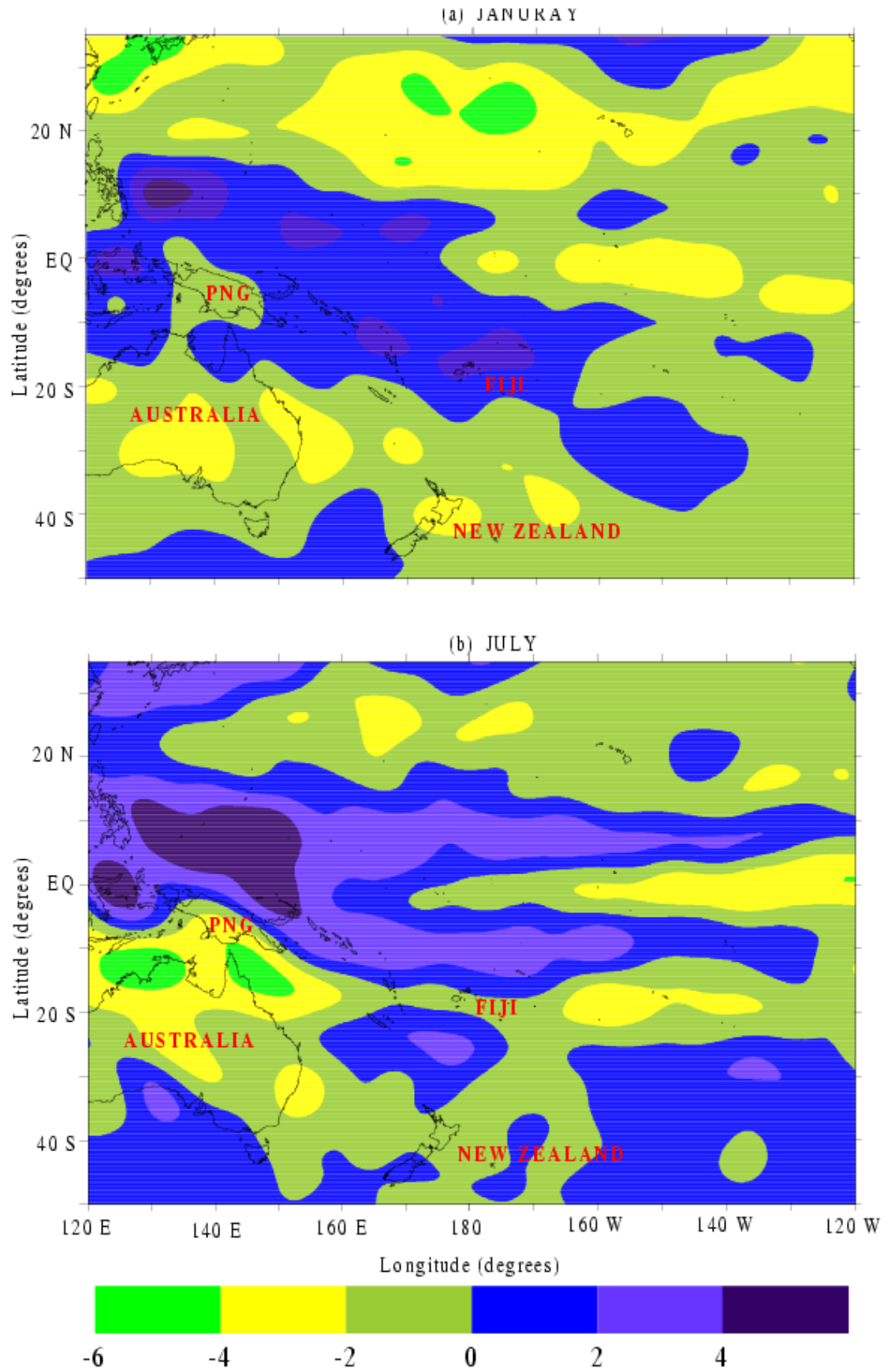
Figure 3.11   Color-coded image of mean horizontal divergence (1990 – 1999) at 200-hPa for the western Pacific region for (a) January and (b) July.
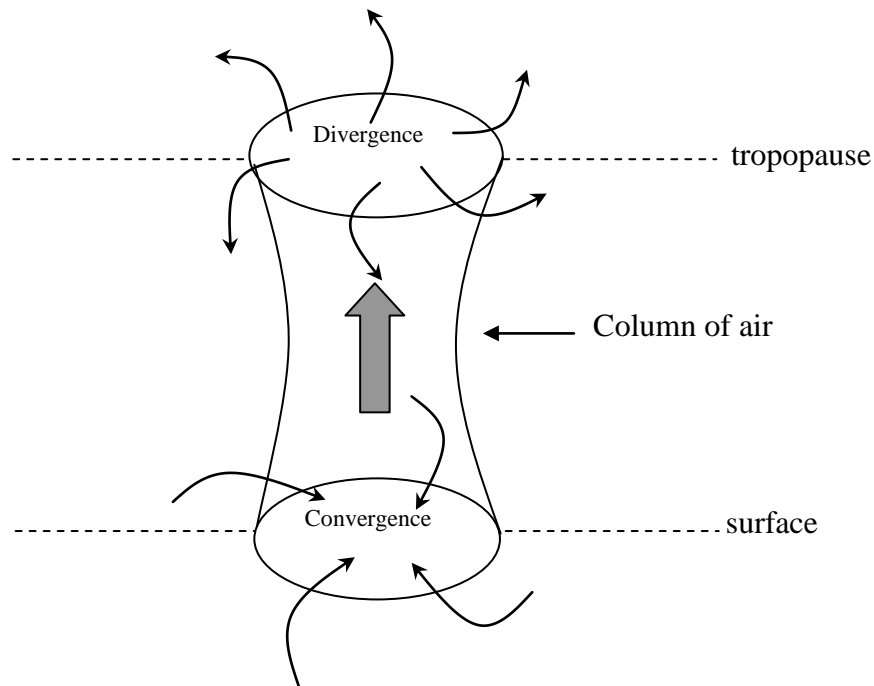
Figure 3.12   Convergence and divergence at the surface and tropopause in a column of air with ascending motion in it (modified after Sturman and Tapper 1996).

3.3.3   Surface Horizontal Divergence and Precipitation Variability

Illustrated in Figure 3.13 are the precipitation patterns and surface divergence fields for the southwest Pacific region during January and July respectively. The unique feature of the pattern during January is the area of maximum precipitation in the central portion of the region, which also coincides with increasingly negative divergence of the flow. Towards the north and south of this, rainfall contours are lower in magnitude and the values of the divergence are less negative. During July, the divergence fields are located more diagonally across the southwest Pacific region but precipitation contours do not follow the divergence fields as closely as they do during January. In the northwestern portion of the central western Pacific region, the divergence values are still quite negative, but precipitation values are lower. This demonstrates that during the month of July, precipitation patterns are not as highly correlated with rainfall as they are during the month of January.

Figure 3.14 shows the surface horizontal divergence fields for the western Pacific and precipitation patterns for western central Pacific region during the summer and autumn.
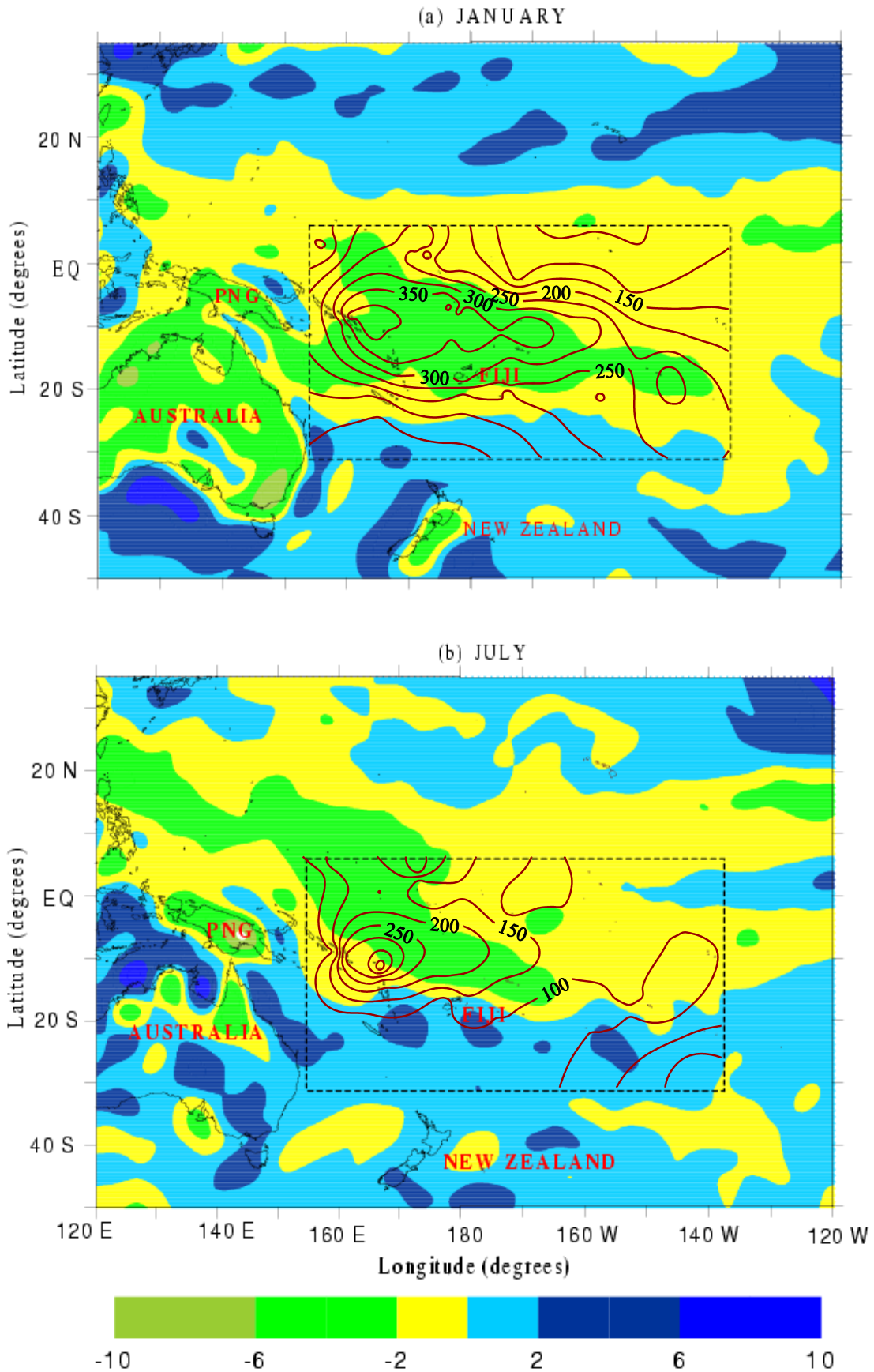
Figure 3.13   Color-coded image of mean surface horizontal divergence (1990 – 1999) ($\times 10^{-6}$ s^{-1}) for the western Pacific region, superimposed on precipitation contours for the southwest Pacific region during (a) January and (b) July.

During summer, precipitation contours show a high degree of spatial correlation with surface horizontal divergence, which is similar to the patterns during January. It is clear from the figure that maximum precipitation values exist in areas of large negative divergence, which are located in horizontal (east-west) position from about 5˚ S – 15˚ S and 150˚ E – 140˚ W. This area of maximum precipitation exists in the central portion of the Pacific region, which includes island groups like Vanuatu, Fiji, Solomon Islands, Tonga, New Caledonia and Western Samoa (see Figure 3.1). Islands located to the eastern side of the region have lower rainfall and show lower degrees of convergence. During autumn, precipitation contours have lower correlation with surface horizontal divergences when compared with summer. However, the central section of the region still maintains high precipitation compared with the whole region, but further to the north where divergences are still negative, precipitation values are lower. The autumn pattern shows that the surface horizontal divergence and precipitation fields have split into two regions, one lying above the equator and the other below the equator. The local minimum in rainfall that occurs at the equator coincides with divergence values that are less negative, hence showing less convergence at the equatorial zone, which has lower rainfall.

Figure 3.15 presents the precipitation and surface horizontal divergence fields during the winter and spring seasons. Both seasons show an increase in precipitation in the regions of highly negative divergence as seen for summer and autumn. Since in the northwestern end of the study region, areas of lower precipitation are seen to coincide with negative divergence, so winter is least correlated with surface horizontal divergence on the spatial scale. During spring, the split in the contours at the equator becomes obvious, which separates the patterns of the northern and southern portion of the central western Pacific region. In the northeastern portion of the region, rainfall values are quite low and this region shows less negative and even positive values of divergence.

3.4 Correlating Precipitation and Surface Horizontal Divergence

Correlation between precipitation and surface horizontal divergence values has been carried out to determine the nature of the linear relationships between them and to quantify the degree of fit to a linear model using the correlation coefficients. In general, mathematically, for any two-sample population, (X and Y), the correlation coefficients are given by
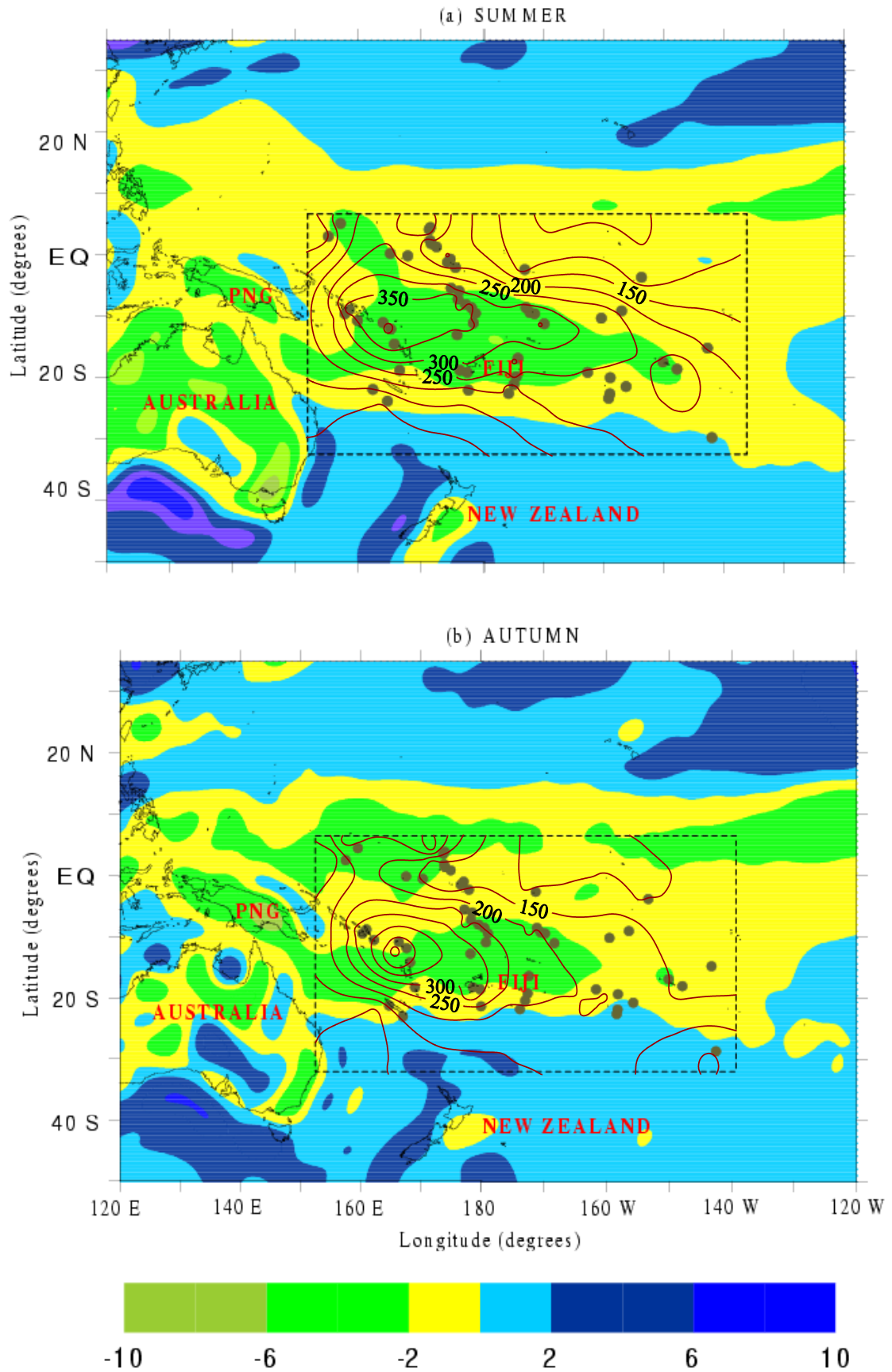
Figure 3.14 Color-coded images of mean surface horizontal divergence (1990 – 1999) ($\times 10^{-6}$ s^{-1}) for the western Pacific region, superimposed on precipitation contours for the southwest Pacific region during (a) summer and (b) autumn.
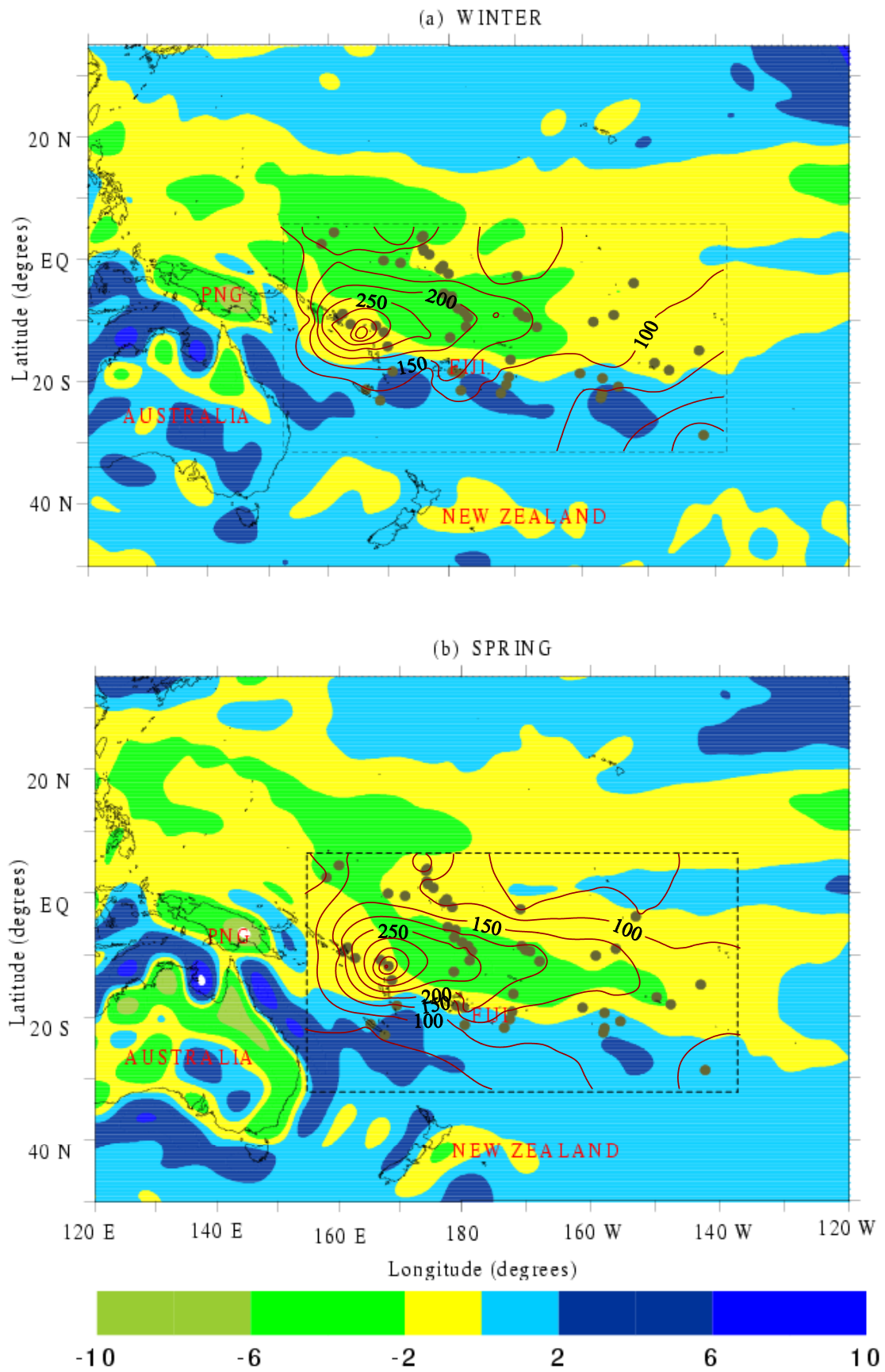
Figure 3.15 Color-coded images of mean surface horizontal divergence (1990 – 1999) ($\times 10^{-6}$ s^{-1}) for the western Pacific region, superimposed on precipitation contours for the southwest Pacific region during (a) winter and (b) spring.

$$r = \frac{C\,(X,Y)}{\sigma_X \sigma_Y} \qquad\qquad [6]$$

where $C\,(X,Y)$ is the covariance between the variables X and Y, which shows the range of the X and Y variables and σ_X and σ_Y are the standard deviations of X and Y.

The gridded precipitation data and surface horizontal divergence values have been correlated at each station for all the seasons. Since some stations are located slightly off the grid points at which the divergence values are located, the nearest value of precipitation to that grid point is considered.

Season	Correlation Coefficient
Summer	- 0.62
Autumn	- 0.22
Winter	- 0.49
Spring	- 0.40

Table 3.2   Correlation coefficients between seasonal surface divergence and precipitation (1990 – 1999).

Illustrated in Figure 3.16a and 3.16b are the correlation plots for summer, autumn, winter and spring. The correlation coefficients are outlined in Table 3.2. Correlation between surface horizontal divergence and precipitation is the highest for summer while for autumn, it is the lowest. This verifies the qualitative interpretation of the superimposed precipitation patterns on the surface divergence plots shown in Figure 3.14. Highest precipitation occurs in the portion of the Pacific region where divergence values are most negative during summer. Precipitation during autumn is the least correlated with surface horizontal divergence. In short, these coefficients show that during summer, surface horizontal
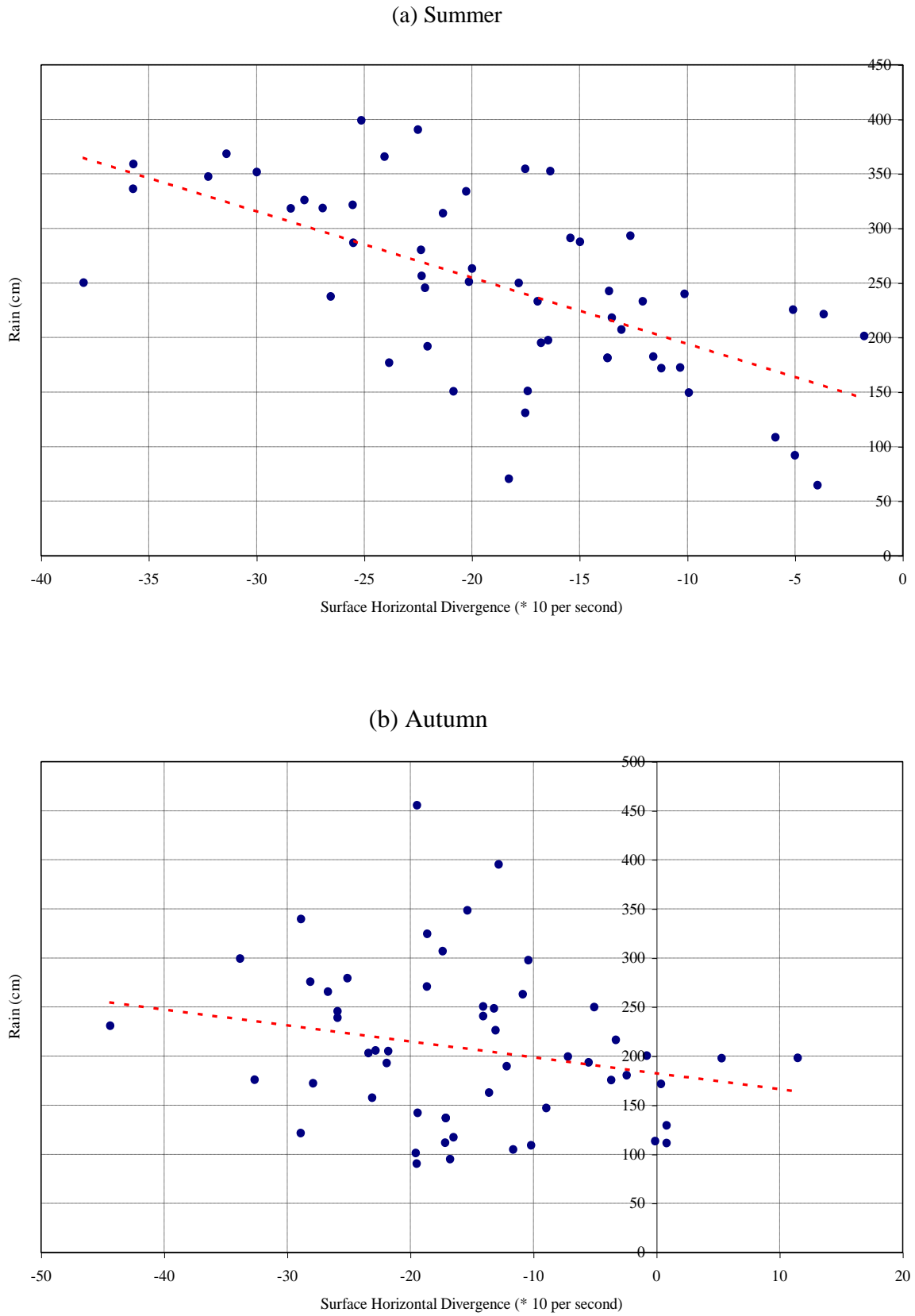
(a) Summer

(b) Autumn

Figure 3.16a Correlation between surface horizontal divergence ($\times 10$ s^{-1}) and rain (cm) from 1990 - 1999 for (a) Summer (b) Autumn.
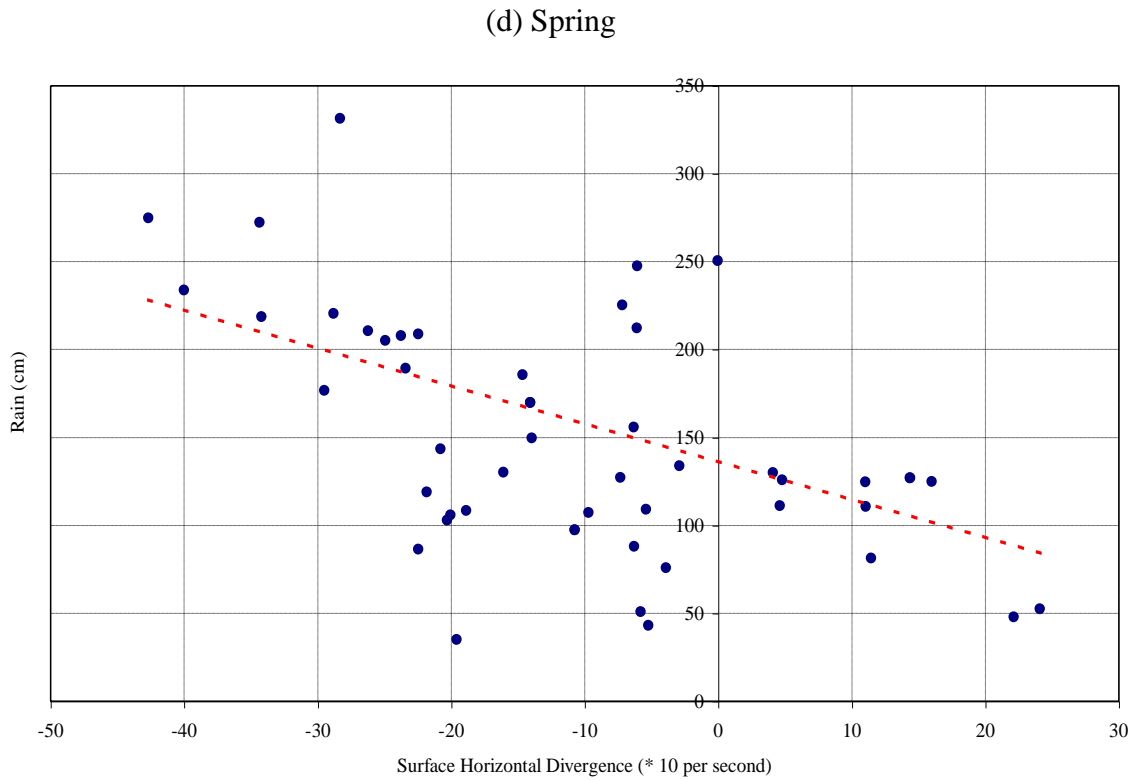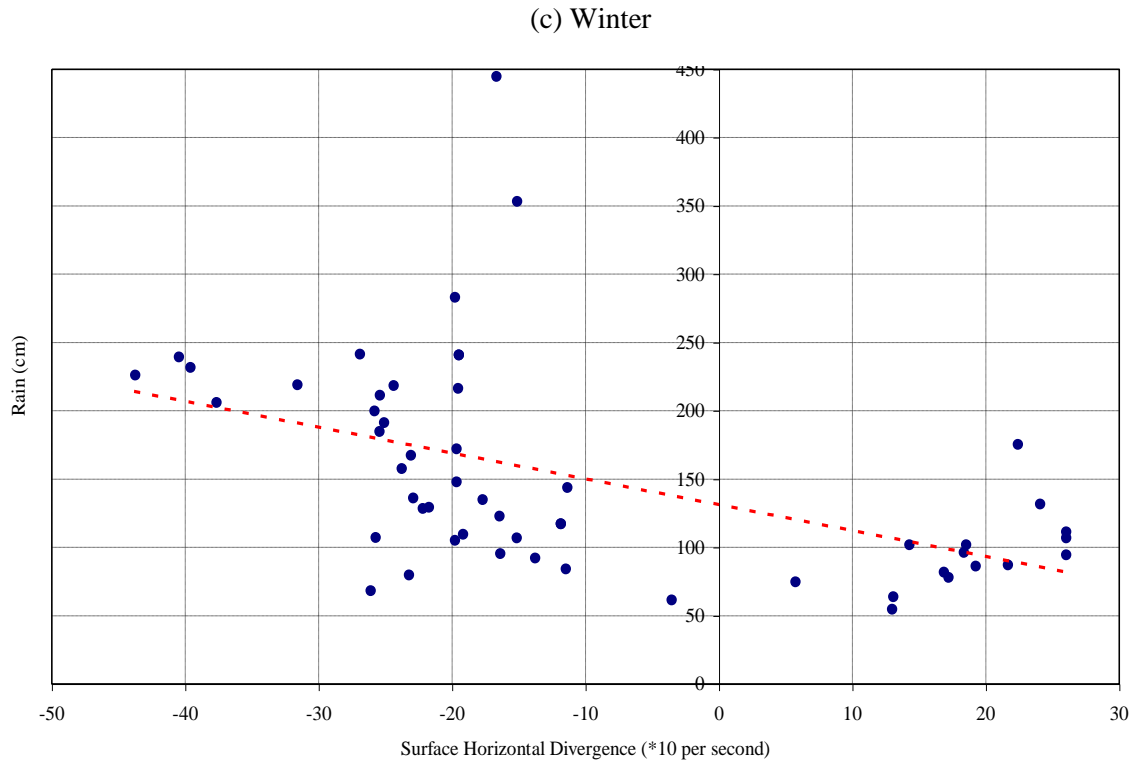
(c) Winter

(d) Spring

Figure 3.16b   Correlation between surface horizontal divergence ($\times 10$ s^{-1}) and rain (cm) from 1990 - 1999 for (a) Winter (b) Spring.

56

divergence is the most significant factor, which affects precipitation when compared with all other seasons. Another analogy of these results would be that during summer, the convergence zone is quite intense and its influence on precipitation is the greatest when compared with all other seasons.

However, Press et al. (1994) outlined a simple method to obtain the significance of a correlation coefficient (r) having a sample size (n), given by the t distribution as

$$t = r \times \sqrt{\frac{n-2}{1-r^2}} \qquad [7]$$

At the 5 % level of significance and n-2 (where n = 53 stations) degrees of freedom, $t_{0.05} =$ 1.675. The following table outlines the t values of the seasonal correlation coefficients and shows whether they are statistically significant at the 5 % level or not.

Season	t - value	Statistically significant or not at the 5 % level
Summer	5.6432	Yes
Autumn	1.6106	No
Winter	4.0142	Yes
Spring	3.1168	No

Table 3.3   Statistical significance of the correlation coefficients between seasonal surface divergence and precipitation.

At the 5 % level, the correlation coefficients for summer, winter and spring are statistically significant while autumn is not. This test verifies that statistically, autumn season is the lowest correlation coefficient between surface horizontal divergence and precipitation. In light of these results, it is fair to conclude that rainfall depends on surface convergence to a significant extent.

3.5 Latitudinal Variation of Precipitation and Surface Divergence

Since the convergence zones vary in latitude, the dependence of precipitation and surface divergence on latitude is investigated. A single longitudinal section of precipitation and surface divergence is considered at $177 \pm 3°$ E since a large number of stations lie within this longitudinal section (Figure 3.1). In this section, the gridded rainfall and surface divergence values are plotted for summer, autumn, winter and spring against latitude and as illustrated in Figures 3.17a and 3.17b. These figures show the local maxima in precipitation at approximately $10 \pm 3°$ S during all seasons except autumn. Consequently, surface horizontal divergence shows local minima around the same latitude. Around $10°$ S, the minima for surface divergence could be due to the location of the SPCZ, which has contributed to the peaks in precipitation at this latitude. Table 3.4a and 3.4b show the seasonal latitudinal position of the maximum and minimum values of rainfall and surface horizontal divergence.

Table 3.4a shows that the peak value of precipitation at the longitude section of $177 \pm 3°$ E occurs at about $9°$ S while it moves further southward to almost $18°$ S during the autumn. In spring, it moves northwards again and is located at $11°$ S. Therefore, the southward shift in precipitation during winter pattern is not well justified using these results. A comparison of the seasonal maximum values of rain shows that the highest rain of 367.98 mm occurs during summer, while the lowest occurs during winter, with autumn and spring having intermediate values.

In Table 3.4b, the latitudinal positions of the minimum values of surface horizontal divergences have been compared during all the seasons. Since during summer, minimum surface divergence occurs at $13°$ S while during winter, it is located at $11°$ S; these results are quite opposite to the one listed in Table 3.4a. As one might expect, maximum rain should occur when surface divergence values are the minimum (most negative). However, this is not true for the analyses presented here. To explain this discrepancy, one must consider the seasonal airflow patterns, which were discussed in the previous section, where it was shown that during winter, the entire wind pattern shifts northwards. Since the wind pattern was located more northwards during winter than during summer, the convergence

(a)

(b)
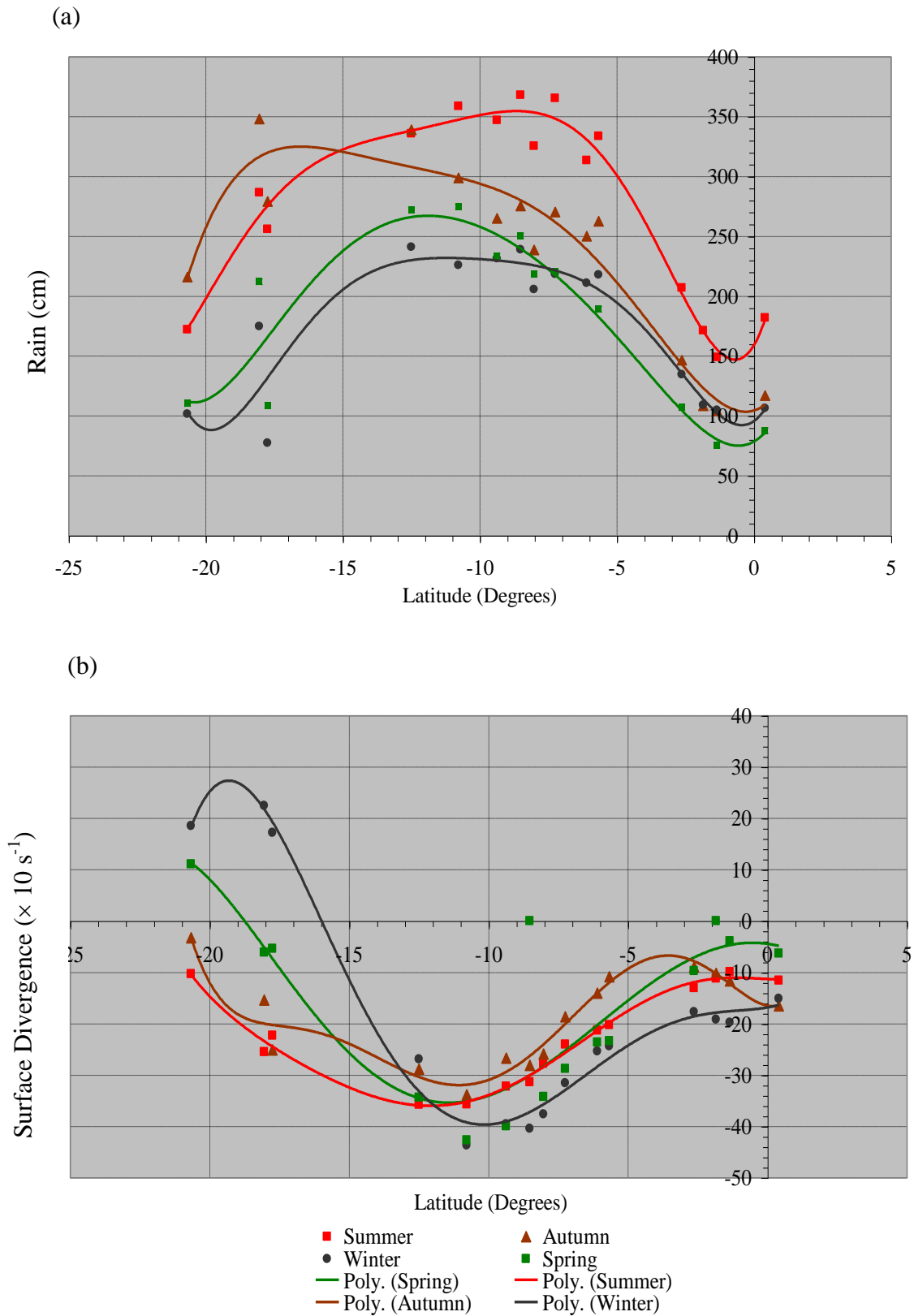
Figure 3.17 Latitudinal variation of (a) rainfall (cm) and (b) surface horizontal divergence ($\times$ 10 s^{-1}) at stations located at 177 $\pm$ 3° E. The polynomial shows the best fit for the points that show trends in precipitation.

Season	Latitudinal Position of Maximum Rainfall	Max Rain Value
Summer	-9	367.93
Autumn	-18	350
Winter	-13	241.01
Spring	-11	274.57

Table 3.4a　　Latitudinal location and value of maximum rainfall (cm) during summer, autumn, winter and spring. Negative latitude denotes south.

zone has also shifted northwards. Consequently, minimum surface horizontal divergence occurs further northwards during winter (at 9° S) than during summer (at 13° S) as one might have expected.

However, by studying the trends in Figure 3.17a and Figure 3.17b, one can conclude that maximum rain and minimum surface divergence, occurs around $10 \pm 3°$ S in the longitude section of $177 \pm 3°$ E. Upon consideration of these results, it is fair to conclude that a rise

Season	Latitudinal Position of Minimum Divergence	Min Divergence Value
Summer	-13	-35.71
Autumn	-11	-33.79
Winter	-11	-40.42
Spring	-11	-42.61

Table 3.4b　　Latitudinal location and value of minimum surface divergence ($\times 10$ s^{-1}) during summer, autumn, winter and spring. Negative latitude denotes south.

precipitation occurs when surface horizontal divergence reaches its minimum (most negative) value while a fall in precipitation occurs when surface horizontal divergence values are a maximum (least negative).

3.6   Correlating ENSO and Precipitation

Since precipitation variability is highly influenced by the ENSO phenomenon (Philander 1990, Vincent 1994, Salinger 1995 and Sturman and Tapper 1996), correlation between the monthly values of the Southern Oscillation Index (SOI) and the rainfall measurements are carried out to determine the inter-relationships between them. The ten-year mean monthly SOI are derived using the SOI data from NIWA. Similarly, the ten-year mean monthly precipitation for the 53 stations is derived using the PACRAIN database, and correlations between the mean monthly SOI and precipitation values are carried out at each station located within the study region. This yields the correlation coefficients at all stations over the region. Since each station has its respective correlation coefficient (or latitude, longitude, coefficient) format, the irregular data is then run through the gridding process to create a homogenous grid of 1.875˚ × 1.875˚. The resulting gridded data is then interpolated and contoured over the study region.

Figure 3.18 represents the spatial correlation (× 100) between the mean monthly precipitation and the SOI for the southwest Pacific. It can be noted clearly that a high degree of spatial correlation exists in the central southwest Pacific, which is located diagonally from the equator to about 20˚ S and between 170˚ E to 145˚ W. Further to the northeast and southwest of the region, correlations are quite small. To explain these results, consider Figure 3.19, which illustrates the mean position of the ITCZ and SPCZ in the Southern Hemisphere. As depicted by the figure, the SPCZ runs diagonally from PNG through to the central southwest Pacific where highly positive correlation exists between precipitation and SOI as shown in Figure 3.18. Because of the presence of the SPCZ, correlation between SOI and precipitation are quite high.

High precipitation occurs during high/positive SOI (i.e. during La Niña conditions) and low precipitation during El Niño conditions along the zone of the SPCZ occurs due to the increase in the intensity of the Hadley Circulation during a La Niña, which tends to favor
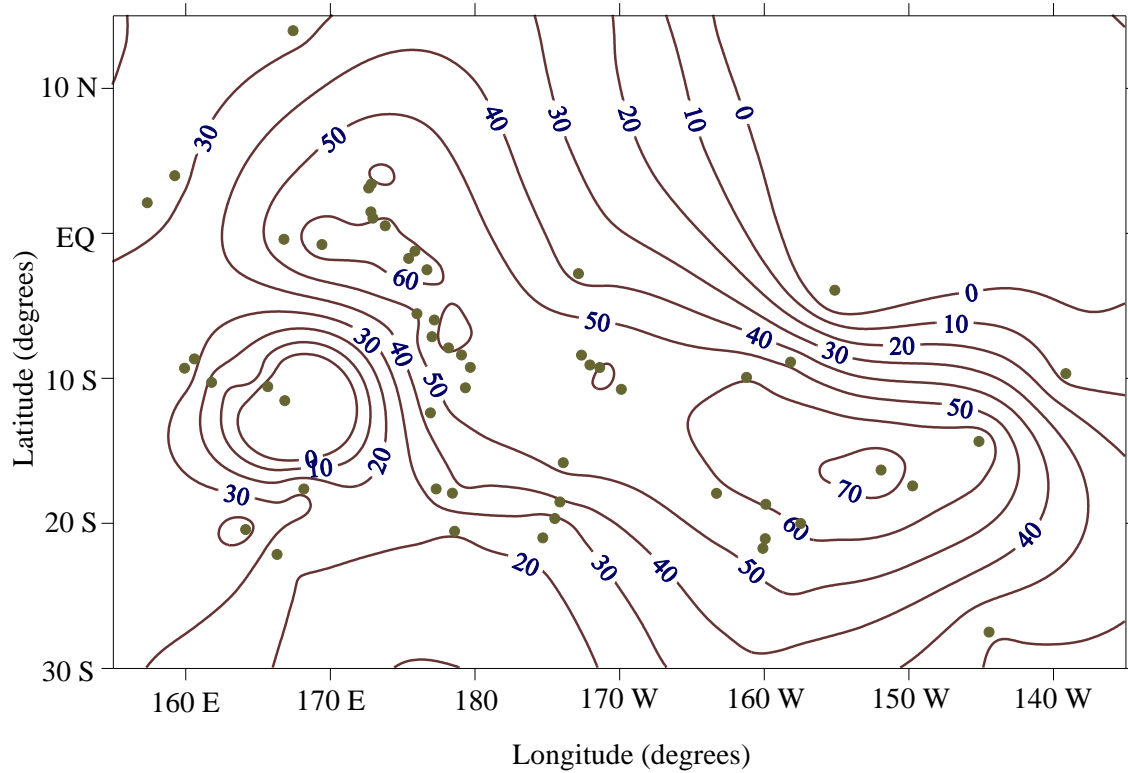
Figure 3.18   Spatial Correlation ($\times$ 100) between monthly precipitation and SOI for the southwest Pacific region at the 5 % level from 1990 – 1999. Station locations are denoted by dots.
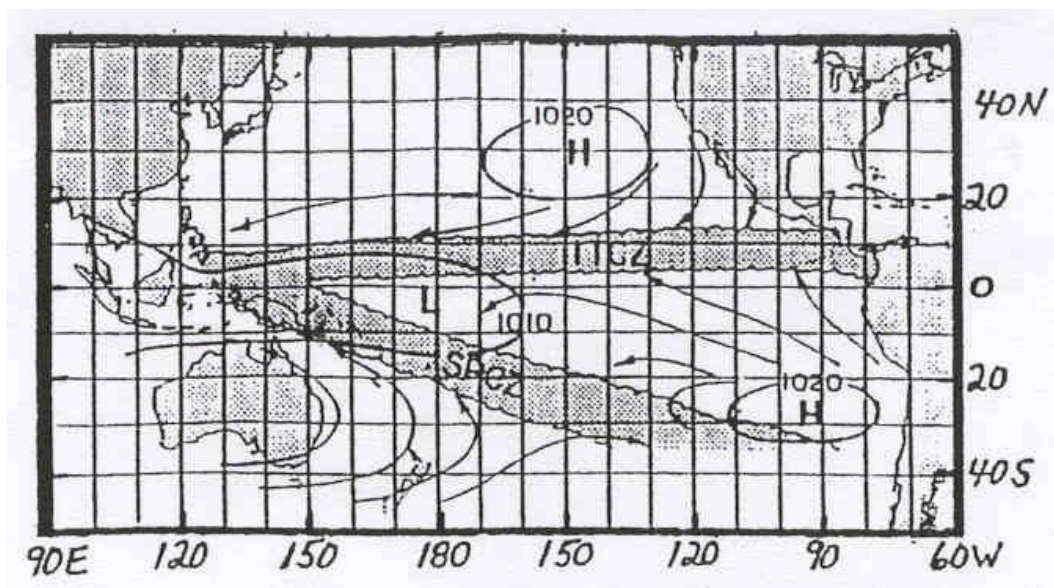
Figure 3.19   Schematic view of the main convergence zone, the ITCZ and SPCZ, along with the mean annual sea level pressure contours and surface wind streams (after Vincent 1994).

precipitation formation along the convergence zone. Basher and Zheng (1998) explained that during a La Niña, Hadley, the Hadley Circulation plays a significant role, while opposite is true for an El Niño event.

3.7   Summary of Main Results

Analysis of the ten-year PACRAIN dataset for the study region has revealed the prominent precipitation patterns that are typical of the islands located within the southwest Pacific. These patterns mark the key months, January to April, as the wettest while May to August are the driest months of the year. Transition to wetter conditions takes place from September to December when the 200 mm isohyet increases its spatial extent over the region. Comparative study of the January and July rainfall fields has shown that the majority of the stations in the study region experience drier periods with the 200 mm isohyets covering relatively a smaller region in July. The seasonal variability shows on overall enhanced precipitation during summer and reduced during winter. The local minimum is located at the equator, with increasing rain to the north and south of the equator.

The wind fields derived from the reanalysis data have indicated the possible positions of the ITCZ and the SPCZ. Converging northeast and southeast trade winds are evident from the wind plots. The illustrations have demonstrated that during January, the possible position of the ITCZ is approximately few degrees north of the equator while during July, it has shifted at least 10˚ northwards. The diagonally located SPCZ emerges from PNG and passes through the western Pacific.

Derived from the wind fields are the color-coded images of the horizontal divergence fields. During January, there are some unexpected large negative divergences of about $(-2$ to $-6) \times 10^{-6}$ s^{-1} over Australia. This can be due to the thermal heating of the continent. However, during January, the image shows that a high degree of convergence is located at about 10 - 15˚ S extending horizontally from 130˚ E to 140˚ W. Conversely, during July, the region of convergence extends from 20˚ N to 20˚ S diagonally across the study region, extending horizontally from 120˚ E to 170˚ W. This shows a slight westward and a significant northward shift of the convergence zone during July. The associated precipitation variability

due to the convergence during summer shows high spatial correlation, while the other three seasons do not show correlation to the same degree.

Correlation coefficients derived between seasonal surface horizontal divergence and precipitation show that summer surface horizontal divergence is the most highly correlated with precipitation while autumn is the least. Precipitation peaks occur at about $10 \pm 3°$ S at the stations located within the longitudinal section of $177 \pm 3°$ E. Consequently, surface horizontal divergence shows the its lowest value (most negative value) at the same latitude. Therefore, highest precipitation occurs when surface horizontal divergence is the most negative, around $10°$ S of the equator. Correlation between mean monthly SOI and precipitation shows a high positive correlation between the two variables.

Chapter 4

Conclusion and Recommendations

4.1 Conclusion

The thesis has investigated a number of aspects of precipitation variability in the southwest Pacific region. Summarized results in Section 3.3 have revealed several features associated with the broad distribution of the ten-year mean precipitation data within the study region. While many of these are similar to previously published literature, others are not. Comparison of the results with those outlined by Basher and Zheng (1998) and Taylor (1973) show that the overall features are quite similar. In particular, January fields show an overall increase in precipitation, while July shows a reduction over the whole region. However, the structure and orientation of the isohyets are different for the results acquired in this study when compared with those presented by Basher and Zheng (1998) and Taylor (1973). This can be attributed to the different gridding processes and smoothing techniques used to present the results. Modelling the precipitation data using OLR as the regression covariant has contributed to the overall smoothness of the isohyets for Basher and Zheng's (1998) presentation. Furthermore, current research is limited to a ten-year dataset while their research was carried out on dataset spanning from 1950 − 1989, which could have caused the discrepancies. Taylor (1973) and Jaeger (1976) also noted the local minimum in precipitation, occurring around the equator. This distinct minimum is a feature during all the months and clearly notable in Figures 3.2 − 3.5. Overall, the irregularly spaced dataset has been used to produce precipitation pattern that are quite plausible.

The wind and surface horizontal divergence fields are comparable to those produced by Rasmusson and Carpenter (1982). These plots have defined the possible positions of the seasonal, January and July convergence zones. Correlation between precipitation and

surface horizontal divergence has demonstrated that summer is the most highly correlated while autumn is the least. As expected, intense differential heating would be the cause of increased precipitation during summer. It was proven that precipitation values are at a maximum where surface horizontal divergence is a minimum, along the longitudinal section of 177 ± 3˚ E. As explained in Rasmusson and Carpenter (1982), large-scale vapor flux convergence rather than local evaporation contributes to enhanced precipitation. This could account for the increased precipitation at minimum values of surface horizontal divergences, where vapor flux convergences are a maximum.

The net southward shift of the local rainfall maxima from summer to winter is yet another feature noted from the analysis and supported by the available literature. However, from the wind and divergence plots, one can note that during winter, the convergence zone moves northwards. This northward movement causes a reduction in precipitation in the central portion of the Pacific, while an increase in the northern portion of the Pacific region. Correlation between SOI and monthly precipitation shows significantly large positive correlation coefficient in the central portion of the study region. Therefore, it is implied that La Niña events contribute significantly towards higher precipitation while El Niño events cause a reduction in the central portion. Coincidentally, this is the typical usual position of the SPCZ, as demonstrated by Figure 3.19. However, further to the northeast and southwest, El Niño effect tends to dominate in enhancing precipitation activities. This result coincides with the annual correlations derived by Salinger et al. (1995) using cluster analysis. However, there are some disagreements between the results and the literature since the coefficients are calculated for monthly and annual timescales respectively.

It should be noted that the analyses are limited to a relatively small precipitation dataset (only 53 stations) and other significant factors such as topography and increased rainfall due to tropical cyclones were neglected. In synopsis, the analysis has given a broad account of precipitation variability and the possible relationships between surface convergence and precipitation in the southwest Pacific region. While it is appreciated that some results are in good agreement with literature, others need to be verified by further in-depth research using datasets that have longer time span. In the next section, some suggestions for further research are provided.

4.2 Recommendations for Future Research

Many issues need to be addressed that could lead to better understanding of precipitation variability within the western Pacific region. Further research suggested by this study include:

- Being volcanic in nature, many islands located within the study region have rugged and high landscapes. Suggestions have been given by authors, e.g. Morrissey et al. (1993) that local terrain factors are significant for larger volcanic islands such as Fiji's Viti Levu, where the prevailing southeast trade winds produce a rainy windward side and a drier leeward side. General Circulation Models (GCM) could provide a better understanding of the associated precipitation variability due to local terrain factors, when run with and without topography.

- It is appreciated that the horizontal divergence fields derived using the wind fields have provided some implications of the existing convergent regions, but long-term composite pictures of satellite imagery could also assist in better understanding of the convergence zones. Some rain and cloud climatologies that currently exist could also be utilized. These could then be used to relate precipitation patterns with the convergence zones.

- The atmospheric boundary layer to be defined more in detail using theoretical and empirical models to study the role of surface and upper air moisture and subsequent momentum transfer in relation to precipitation variability.

- In situ and satellite derived precipitation data could be merged to produce larger datasets for the southwest Pacific region with greater spatial resolution. Currently available data are limited to station observations, which are quite sparse so interpolations between them are unrealistic over the vast expanse of the ocean where it is impossible to take measurements. Larger datasets derived from satellites could be a solution to this problem.

Appendix A

Acronyms

ENSO	El Niño Southern Oscillation
EVAC	Environment Verification and Analysis Center
ITCZ	Inter-tropical Convergence Zone
MSLP	Mean Sea Level Pressure
NCC	National Climate Center
NCEP/NCAR	National Center for Environmental Prediction/National Center for Atmospheric Research
NIWA	National Institute of Water and Atmospheric Research
NOAA	National Oceanic and Atmospheric Administration
OLR	Outgoing Longwave Radiation
PACRAIN	Pacific Comprehensive Rainfall
SOI	Southern Oscillation Index
SPARCE	School of Pacific Rainfall Climate Experiment
SPCZ	South Pacific Convergence Zone
SST	Sea Surface Temperature

Appendix B

Matlab Programs

Sample subroutines used to calculate divergence at the 200-hPa level using zonal and meridional wind data.

```matlab
% This program calculates the divergence for January 1990-1999
% at 200 hPa.

clear;

fid0=fopen('C:\shakeel\Div Fields\DivJan10m.txt','w');
loc = load('c:\matlab\bin\location.txt');
value = load('C:\shakeel\Winds\Surface\Winds10m.txt');

n=2;
m=1;

delta_Y=6372000*(2.5*pi/180);

for p=1:17662
    v2=value(n,2);
    v1=value(n+384,2);

    u1=value(m+192,1);
    u2=value(m+192+2,1);

    lat=loc(n+192,2);
    delta_X=6.375e6*(cos(pi*lat/180))*(1.875*pi/180);
    diverg(p) = 1000000*(((u2-u1)/(2*delta_X))+((v2-
    v1)/(2*delta_Y)));

    n=n+1;
    m=m+1;
end

d=0;
a=145;

for p=1:17662
a=a+1;
d=d+1;

fprintf(fid0,'   %5.2f        %5.2f         %5.2f', loc(a,1),
loc(a,2), diverg(d));
```

```matlab
fprintf(fid0,'\n');
end



fclose(fid0);



% This program calculates Divergence Fields for July 1990-1999
% at 200 hPa

clear;

fid1=fopen('C:\shakeel\Div Fields\DivJul10m.txt','w');
loc = load('c:\matlab\bin\location.txt');
value = load('C:\shakeel\Winds\Surface\Winds10m.txt');

n=2;
m=1;

delta_Y=6372000*(1.875*pi/180);

for p=1:17662
     v2=value(n,12);
     v1=value(n+384,12);

     u1=value(m+192,11);
     u2=value(m+192+2,11);

     lat=loc(n+192,2);
     delta_X=6.375e6*(cos(pi*lat/180))*(1.875*pi/180);
     diverg(p) = 1000000*(((u2-u1)/(2*delta_X))+((v2-
     v1)/(2*delta_Y)));

     n=n+1;
     m=m+1;
end

d=0;
a=145;

for p=1:17662
a=a+1;
d=d+1;

fprintf(fid1,'    %5.2f        %5.2f        %5.2f', loc(a,1),
loc(a,2), diverg(d));
fprintf(fid1,'\n');
end



fclose(fid1);
```

Bibliography

Basher, R.E., Collen, B., Fitzharris, B., Hay, J., Mullan, B. & Salinger, M.J. (1992), '*Preliminary Studies of South Pacific Climate Change*' New Zealand Meteorol. Service, Wellington, 70 pp

Basher, R.E., Zheng, X. (1998), '*Mapping Rainfall Fields and their ENSO Variation in Data-Sparse Tropical Southwest Pacific Ocean Region*', Int. J. Climatology, **18**, 237-251

Bjerknes, J. (1969), 'Atmospheric Teleconnections from the Equatorial Pacific', Mon. Wea. Rev., **97**, 163-192.

Brown, R.A. (1991), '*Fluid Mechanics of the Atmosphere*', Academic Press, London, UK.

Coughlon, M.J., Tapp, R. & Kinninmonth, W.R. (1990), '*Trends in Australian Temperature Records*', Draft Contribution to IPCC, WG1, Sec. 7

Cressie, N.A.C. (1991), '*Statistics for Spatial Data* ', John Wiley and Sons, Inc., New York, 900 pp.

Curtis, S. & Adler, R. (2000), '*ENSO Indices Based on Patterns of Satellite-Derived Precipitation*', J. Climate, **13**, 2786-2793

Dorman, C.E. (1979), '*Precipitation over the Pacific Ocean*', Mon. Wea. Rev., **107,** 896-910

Eischeid, J.K., Baker, C.B., Karl, T.R. & Diaz, H.F. (1995), '*The Quality Control of Long-Term Climatological Data Using Objective Data Analysis*', J. Appl. Meteor., **34**, 2878-2795

Folland, C.K., Karl, T.R., Nicholls, N., Nyenzi, N., Parker, D.E. & Vinnikov, K.Y. (1992), 'Observed Climate Variability and Change', in Houghton, J.H., Callander, B.A. & Varney, S.K. (eds.), '*Climate Change 1992: The Supplementary Report to the Scientific Assessment*', Cambridge University Press, Cambridge, 135-170

Gates, W.L., Henderson-Sellers, A., Boer, G.J., Folland, C.K., Kitoch, A., McAvaney, B.J., Semazzi, F., Smith, N., Weaver, A.J. & Zheng, Q-C. (1995), Climate Models – Evaluation, in '*Climate Change 1995: The Science of Climate Change, IPCC Second Assessment Report*', Cambridge University Press, Cambridge, 229-284

Hartmann, D.L. (1994), '*Global Physical Climatology*', Academic Press, London, UK.

Hastenrath, S. (1991), '*Climate Dynamics in the Tropics*', Kluwer Academic Press, Netherlands

Holton, J.R. (1992), '*An Introduction to Dynamical Meteorology*', Academic Press, Inc

Houghton, J.H., Callander, B.A. & Varney, S.K. (1992), '*Climate Change 1992: The Supplementary Report to the IPCC Scientific Assessment*', 200 pp.

Hubert, L.F. (1961), '*A Sub-tropical Convergence Line of the South Pacific: A Case Study using Meteorological Satellite Data*', J. Geophy. Research, **66**, 797-812

Hulmes, M. (1992), '*A 1951-80 Global Land Precipitation Climatology for the Evaluation of General Circulation Models*', Climate Dynamics, **7**, 57-72

Hulmes, M. (1994), '*Validation of Large-Scale Precipitation Fields in General Circulation Models, Global Precipitation and Climatology Change*', M. Desbois and F. Desalmand, Eds., NATO ASI Series, Springer-Verlag, 387-406

Janowiak, J.E., Arkin, P.A. & Xie, P. (1995), '*An Examination of the East Pacific ITCZ Rainfall Distribution*', J. Climate, **8**, 2810-2823

Kaladis, G.N., Storch, H.Von., & Loon, H.Van. (1989), '*Origin of South Pacific Convergence Zone*', J. Climate, **2**, 1185-1195

Kalnay, E.M. Kanimatsu, Kistler, R., Collins, W., Daven.D, Grandin, L., Iredell, M., Saha, S., White, G., Wollen, J., Zhu, Y., Chelliah, M., Ebisuazaki, W., Higgins, W., Janowiak, J. (1996), '*The NCEP/NCAR 40 – yr Reanalysis Project*', Bull. Am. Soc., **77**, 437-471 plus CD-ROM

Khatep, M. (1982), '*Precipitation Climatology of the Southwest Pacific in Relation to Upper to Parameters – PhD Thesis in Geography* ', University of Otago, Dunedin, New Zealand

Keckler, D. (1994), '*Surfer for Windows: Contouring and 3D surface Mapping*', Golden Software, Inc., USA

Linacre, E. (1992), 'Climate Data and Resources: A Reference Guide', Roultadge, London, UK

McHugh, M.J. (1999), '*Precipitation over Southern Africa and the Global-Scale Atmospheric Circulation During Boreal Winter – A dissertation presented for PhD in Geography* ', The Ohio State University

Mirsky, N. (2000), '*QC of the PACRAIN Daily Rainfall Database*', The University of Oklahoma, USA

Morrissey, M.L. (1986), '*A Statistical Analysis of the Relationships among Rainfall, Outgoing Longwave Radiation and the Moisture Budget during January-March 1979*', Mon. Wea. Rev. **114**, 930-942

Nicholls, N. & Lavery, B. (1992), '*Australian Rainfall Trends During the Twentieth Century*', Int. J. Climatol., **12**, 153-163

Oort, A. & Yienger, J. (1996), '*Observed inter-annual Variability in the Hadley Circulation and its Connection to ENSO*', J. Climate, **9** (11), 2751-2767

Peixoto, J.P., & Oort, A.H. (1992), '*Physics of Climate',* Amer. Instit. Phys., New York, USA

Philander, G.S. (1998), '*Learning from El Niño*', Weather, **53** (9), 271-337

Philander, G.S., Halpern, D., Lambert, G., Lau, N-C., Li, T. & Pacanowski, R.C. (1996), '*Why the ITCZ is Mostly North of the Equator*', J. Climate, **9**, 2958-2971

Philander, S.G. (1990), '*El Niño, La Niña and the Southern Oscillation',* Academic Press, London, UK

Pittock, A.B. (1975), '*Climate Change and Patterns of Variation in Australian Rainfall'*, Search, **6**, 498-504

Plummer, N. (1991), '*Annual Mean Temperature Anomalies over Eastern Australia'*, Bull. Aust. Meteorol. Oceanogra. Soc., **72**, 42-44

Press WH, Flannery BP, Teukolsky SA, and Vetterling WT. (1994), "*Numerical recipes in Pascal*", Cambridge University Press ISBN 0-521-37516-9. p.189

Ramage, C.S. (1971), '*Monsoon Meteorology*', New York and London, Academic Press

Ress, D.G. (1985), "*Essential Statistics",* London and New York, Oxford Polytechnic, UK.

Riehl, H. (1979), '*Climate and Weather in the Tropics*', Academic Press, London, UK

Salinger, M.J. & McGlown, M.S. (1990), '*New Zealand Climate: The past two million years'*, New Zealand Climate Record 1990, Royal Society of New Zealand Bulletin, **28**, 13-18

Salinger, M.J., McGann, R., Coutts, L., Collen, B. & Fouhy, E. (1992a), '*Temperature Trends in New Zealand and Outlying Islands 1920-1990*', New Zealand Meteorol. Soc., Wellington, 46 pp

Salinger, M.J., McGann, R., Coutts, L., Collen, B. & Fouhy, E. (1992b), '*Rainfall Trends in New Zealand and the Outlying Islands 1920-1990*', New Zealand Meteorol. Soc., Wellington, 33 pp

Salinger, M.J. (1995), '*Southwest Pacific temperatures: Trends in maximum and minimum temperatures*', Atmos. Research, **37**, 87-99

Salinger, M.J., Basher, R.E., Fitzharris, B.B., Hay, J.E., Jones, P.D., Macveigh, J.P. & Schmidely-Leleu, I. (1995), '*Climate Trends in the Southwest Pacific'*, Int. J. Climatology, **15**, 285-302

Salinger, J.M, Rob, A., Bindoff, N., Hannah, J., Lavery, B., Lin, Z., Lindesary, J.,Nicholls, N., Plummer, N., & Torok, S. (1996), in '*Greenhouse – Coping with Climate Change', 'Observed Variability and change in Climate and sea level in Australia, New Zealand and the South Pacific',* Jointly by CSIRO Division of Atmospheric Research and National Institute of Water and Atmospheric Research, NIWA

Spencer, R.W. (1993), '*Global Oceanic Precipitation from the MSU during 1979-1991 and Comparisons to Other Climatologies'*, J. Climate, **6**, 1301-1326

Steiner, J.T. (1980), '*The Climate of the Southwest Pacific Region: A Review for Pilots* ', New Zealand Meteorol. Service Miscellaneous Publication 166, Wellington, 35 pp

Steiner, J.T. (1981), '*The Climate of the Southwest Pacific Region'*, New Zealand Meteorological Service Miscellaneous Publication No 166, Govt. Printer, New Zealand

Sturman, A.P. & Tapper, N.J. (1996*), 'The Weather and Climate of Australia and New Zealand'*, Oxford University Press, Oxford, UK

Sturman, A.P. & McGowan, H.A. (1999), Chapter One: Climate in '*The Pacific Islands: Environment and Society*', Bess Press, Hawaii, 3-18

Sumner, G. (1988), *'Precipitation – Process and Analysis',* The Bath Press, Great Britain
Taylor, R.C., (1973), '*An Atlas of Pacific Island Rainfall*', Data Report 25, HIG-73-9, Hawaii Institute of Geophysics

Thompson, R.D. (1998), '*Atmospheric Process and Systems',* Roultadge, London, UK.

Ushiyama, T., Satoh, S. & Takeuchi, K. (1995), '*Time and Spatial Variations of Mesoscale Rainfalls and their Relationship to the Large-Scale Field in the Western Pacific*', J. Met. Soc. Japan, **73**(2B), 379-392

Vincent, D.G. (1994), '*The South Pacific Convergence Zone: A Review*', Mon. Wea. Rev., **122**, 1949-1969

Wallace, J.M., & Hobbs, P.V. (1977), '*Atmospheric Science – An introductory Survey'* Academic Press, London, UK

Zheng, Q., Yan, X.H., Liu, W.T., Tang, W. & Kurz, D. (1997), '*Seasonal and Inter-annual Variability of Atmospheric Convergence Zones in the Tropical Pacific observed with ERS-1 Scattermeter*', Geophys. Res. Lett., **24**, 3, 261-263

Zheng, X. & Basher, R. (1995), '*Thin-Plate Spline Modeling of Spatial Climate Data and its Application to Mapping South Pacific Rainfalls*', Mon. Wea. Rev., **123**, 3086-3102

Zillman, J.W., Downey, W.K. & Manton, M.J. (1989), '*Climate Change and its Possible Impacts on Southwest Pacific Region, Scientific lecture presented at the tenth session of WMO regional association V,*', Singapore, 69 pp